Solar Energy 301 (2025) 113878

Contents lists available at ScienceDirect

Solar Energy

journal homepage: www.elsevier.com/locate/solener

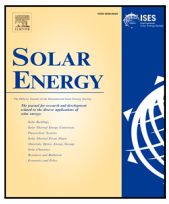

Comparison of conventional and simple artificial neural network models for high-performance separation of global solar irradiance components at minutely resolution

Jose A. Ruiz-Arias [a,*], Enrique Domínguez [b], Christian A. Gueymard [c]

[a] Department of Applied Physics I, Faculty of Sciences, University of Malaga, Campus Teatinos s/n, Malaga, 29071, Spain
[b] Department of Computer Languages and Computer Science, University of Malaga, Bulevar Louis Pasteur 35, Malaga, 29071, Spain
[c] Solar Consulting Services, Colebrook, NH 03576, USA

ARTICLE INFO

Keywords:
GHI component separation
Conventional separation models
Artificial neural network models
Machine learning
Model benchmark

ABSTRACT

Solar radiation components are required by most solar applications, but global horizontal irradiance (GHI) is the only measurement or model output that is usually available. Empirical component separation models separate GHI into its components and are the only practical solution that can ensure the availability of the solar components on a global scale. The growing availability of public observed datasets and the rise of machine learning (ML) have paved the way for a new modeling framework, where conventional and ML-based models now coexist. Many ML techniques have been proposed so far, but they have not been clearly found to improve the best conventional models on a global scale. Moreover, the complexity of some ML approaches is out of the reach of normal users, which is detrimental to their practical adoption in regular applications. This study investigates whether a basic artificial neural network (ANN) with a reduced number of easily accessible input variables can outperform the best conventional separation models on a global scale. Three ANN versions with different input combinations are tested using a global database of 117 radiometric stations, and are evaluated against 13 of the best conventional models. Although two of the ANN models are not conclusively better than the best conventional separation model, proving that ML-based models are not necessarily better than conventional models, the third one is consistently better at nearly all ground sites, reducing the average root mean square error of the predicted direct normal irradiance from ≈16% with the best conventional model to ≈14%.

1. Introduction

Solar applications are ultimately sustained by solar radiation, which is the principal energy factor determining their performance. Thus, a detailed quantitative and qualitative knowledge of the local solar resource is necessary, which also includes the precise separation of total solar irradiance into its direct and diffuse components. The direct component is traditionally measured in the normal direction to the Sun, thus being customarily referred to as direct normal irradiance (DNI), and is the main driver in concentrating solar applications [1,2]. In contrast, planar photovoltaic applications require both DNI and diffuse horizontal irradiance (DIF), from which both the total solar irradiance incident on a horizontal surface (GHI) and on the tilted plane of the photovoltaic array are evaluated [3–6]. However, independent measurements of DNI and DIF are scarce and much less common than those of GHI because they involve more sophisticated, expensive, and delicate instruments, as well as more stringent maintenance protocols [7]. In parallel, most satellite-based solar resource databases, which constitute an essential part of any solar resource assessment, can evaluate GHI from satellite imagery [8], but not their DNI and DIF components. In such a context, methods to separate the observed or modeled GHI into its DNI and DIF components are required to make full use of the available GHI data streams.

Alternatively, DNI and DIF could be directly evaluated from radiative transfer models that are based on universal physical principles. However, they require a description of the atmosphere that is rarely available, either because the relevant atmospheric variables are not all known or because they are known with insufficient accuracy. This is typically the case for variables related to cloudiness. Moreover, the usage of physical atmospheric models is cumbersome and requires considerable computing resources that are usually beyond the reach of solar engineers in their daily practice [9]. In this context, GHI component-separation models—hereafter, separation models—have been widely

* Corresponding author.
E-mail addresses: jararias@uma.es (J.A. Ruiz-Arias), enriqued@lcc.uma.es (E. Domínguez), chris@lsolarconsultingservices.com (C.A. Gueymard).

https://doi.org/10.1016/j.solener.2025.113878
Received 17 April 2025; Received in revised form 28 July 2025; Accepted 12 August 2025
Available online 15 September 2025

used wherever ground-based observations of components are permanently or temporarily unavailable and physical modeling is not feasible [10]. This is the case virtually everywhere because observations of solar components and/or of atmospheric constituents for physical modeling are rarely available at the specific sites of interest, which leaves empirical separation methods as the only possible practical approach.

Traditionally, separation models have been composed of three tightly integrated elements: (1) a primary transfer function with adjustable coefficients, (2) a set of explanatory variables that are ideally accessible everywhere, and (3) an empirical fitting method using observations from a few sites to adjust the coefficients. This empirical structure has traditionally made these models inherently local and somewhat lacking in generalization. However, it is worth noting that element (2) should always be a primary design constraint to ensure the global scope of the separation model. Otherwise, it would suffer from similar issues as physical models. In contrast, improvements in elements (1) and (3), which are related to model complexity and training scope, respectively, constitute the main current research trends to improve separation models, which have been favored by the increase in the number of available public radiometric sites and the rise of artificial intelligence (AI) and machine-learning (ML) methods. It is worth mentioning also that the temporal resolution of interest for separation models has historically evolved throughout the last six decades from monthly or daily, through hourly, and, since the 2010s, minutely. The reason, apart from the increase in instrumental, computational, and financing resources, is that photovoltaic (PV) solar power production is vulnerable to rapid solar radiation fluctuations originating mainly from transient clouds [11,12]. The intensity and frequency of these fluctuations, which are barely detectable if the temporal resolution is longer than ≈5 min [13], need to be taken into account at the design stage of PV systems [14,15].

The evolution just discussed explains why many new 1-min separation models have been introduced since Engerer's, published in 2015 [16], although the very first study on 1-min separation modeling actually dates back to 1988 [17]. The most notable state-of-the-art 1-min separation models have been extensively discussed and tested in prominent works of the literature [10,18,19]. However, in parallel to the evolution toward fine-scale separation, new ML-based models have been steadily proposed. For instance, Aler et al. [20] used the predictions of 140 conventional separation models, most of them designed for hourly data, as inputs to an extreme gradient boosting model (XGB) [21] to separate 1-min GHI observations at 54 radiometric stations worldwide. They found that a pool of only 26 of these conventional separation models was sufficient to significantly improve their individual results, as was also the case when directly training the XGB model with a set of 14 explanatory variables of those used by the conventional separation models, which reduced the average root mean square deviation (RMSD) of DNI from ≈27% with the best separation models at each site to ≈19% with the XGB model. More recently, Ramadhan et al. [22] tested five ML techniques, among which support vector regression was the best performer, to separate the GHI components using six atmospheric inputs, including relative humidity, dew point and dry bulb temperatures, wind speed and cloud amount. Overall, these inputs help to improve the performance of the models, but at the cost of restricting their application scope to only places and situations in which such observations are available. Furthermore, the study was conducted at a single location in South Korea, which prevents any conclusion about the potential universality of the results. Later, using data from that specific station [22], and thus sharing the same locality issue, Rajagukguk and Lee [23] obtained the best results with long-short-term memory models, also evaluated in [22], at various temporal resolutions from 1 min to 1 h. In a subsequent work, the same authors used data from 10 BSRN stations to train and validate three boosting-based ML approaches, obtaining the best results with a 9-parameter CatBoost model [24]. Oh et al. [25] used data from 20 stations in temperate areas and 5 stations in South Korea to train light gradient boosting, XGB, and artificial neural network (ANN) models. The latter outperformed the other two ML approaches, the Aler et al. [20] ML-based approach discussed above, as well as a collection of 21 conventional separation models. All these results highlight a typical finding in studies involving separation modeling with ML-based techniques, to the effect that it is not easy to establish a consistently best-performing technique.

An additional specific aspect discussed in the literature is the generalizability of ML-based models. For instance, Rodríguez et al. [26] has recently discussed the generalization achieved by a deep neural network (DNN) model when trained to separate 1-min GHI observations, in this case, using observations from 49 radiometric stations along five climate zones. In particular, multiple versions of the DNN model were trained for each climate zone using data from a single radiometric site at a time and validated with data from the remaining sites for that climate zone. The authors hypothesize that the level of generalization achieved by DNNs can be assessed on the basis of the best performing model in each climate zone, concluding that DNN-based separation models can be considered universal, or "quasi-universal". The generalizability of DNNs, however, is conditioned by the number of sites selected for training (in this case, only one site). Local data subsampling could seriously limit the desired universality. In contrast, Ruiz-Arias and Gueymard [19] have conducted a benchmark analysis based on data from more than 100 radiometric sites from all continents, where data from about half of the sites were used, to a greater or lesser extent, to train the benchmarked models, and the data from the other half remained unseen for all models, with the only exception of Yang5 [27]. The models are thus trained using data from multiple locations and validated at unseen locations on a global scale. Overall, the benchmark comprises 13 conventional separation models for 1-min GHI observations, including four versions of the very recent GISPLIT separation model [28], two of which use XGB to separate GHI under highly variable sky situations [29], the most challenging situations for separation models. Overall, the climate-agnostic GISPLIT version, assisted with XGB, was the best, or nearly the best, performer in all climate zones, thus being promulgated as the best universal separation model out of this benchmark pool.

In a more ambitious study aiming to compare conventional and ML-based separation models, Chu et al. [30] compared 10 conventional state-of-the-art and 10 ML-based separation models using 5 years of data, but only at 12 radiometric stations. Data from 7 radiometric stations were used to train and validate the models, while the remaining three were kept for independent evaluation. The study found that, on average, the site-wise error of the ML models is from 15.2% to 22.6% lower than that of the conventional models at training locations and from 7.9% to 17.6% lower at unseen locations, concluding that "data-driven models demonstrate enhanced overall performance" (over conventional models). Although this might be true, some important aspects were apparently overlooked there. In particular, the results revealed that Yang4, the conventional model with the smallest RMSD at the sites used to train the data-driven models, has higher RMSD than the best data-driven model (XGB). However, the results are surprisingly reversed at the three unseen sites, that is, Yang4 has RMSD smaller than XGB, indicating probable overfitting and/or lack of generalization in the latter, provided that the data from the training and the validation sites have similar statistical properties, as expected.

Just recently, a novel and extremely convoluted deep-learning approach, IIF-IMCSM, has been proposed, which combines multiple convolutional neural networks and other AI techniques [31]. It has shown some accuracy gain over conventional and ML-based separation models, which are otherwise much simpler, easily reproducible, and portable. However, the modest improvement in model accuracy does not appear to justify the massive increase in complexity, which further prevents any subsequent replication by potential users, all the more so that its code, or even a binary file, has not been made publicly available, to the best knowledge of these authors. This raises an

important question about the real impact of any such complex model, which is in practice a black box that cannot be tested or reproduced by real users. Just like with physical models, an excessive complexity can prevent or restrict the use of the model in real applications.

In general, more global benchmark studies of conventional and ML-based separation models are needed, particularly to address the question of whether the best conventional separation models can be surpassed by universal ML-based approaches. In this sense, it is important to emphasize that ML models must always follow three design principles: (1) limited complexity to guarantee widespread adoption in real applications, (2) the use of a limited set of explanatory variables that are easily accessible everywhere, and (3) the use of a training dataset on a global scale. Only these three principles combined can guarantee true model universality, which must consider not only global coverage (second and third principles), but also a global user reach (first principle). Moreover, considering that (2) is an inviolable principle, the gain in accuracy resulting from an increase in model complexity might not be significant or might occur at the expense of excessive loss of usability.

This contribution aims at providing a global benchmark for conventional and ML-based separation models that draws conclusions about the most suited universal approach subject to the three previous design principles. To do so, only ANN models with simple and easily reproducible architectures are considered, using a set of only three explanatory variables, typically used in component separation modeling, over a worldwide radiometric dataset made up of 117 ground stations across all continents.

2. Observational database

The observational database includes measurements of GHI, DIF, and DNI with minutely resolution from 117 research-class stations that belong to two distinct datasets and have already been used in a previous study [28], to which the interested reader is referred for more details. Here, only a brief summary is presented for conciseness.

The first dataset is made up of 52 stations from the Baseline Surface Radiation Network [BSRN, 32] with 5 calendar years of data per station (except for two of them, Petrolina in Brazil and Solar Village in Saudi Arabia, which both have only four years of data). This dataset is divided into a subset for model validation, hereafter referred to as Valid dataset, which is made up of the data from the last calendar year at each radiometric station, and a subset for model training, hereafter referred to as Train dataset, which is made up of the remaining four years of data at each radiometric station. With respect to the original dataset [28], two stations (Lerwick and Camborne in the United Kingdom) are excluded here because too many observations from their respective validation years were flagged during the preliminary data quality control process.

The second dataset is made up of 65 stations from various public and private stations put together through a collaborative effort of the Solar Resource for High Penetration and Large-Scale Applications Working Group of the International Energy Agency's Photovoltaic Power Systems (PVPS) Program Task 16. This dataset, whose sites are not collocated with the sites in the Train or Valid datasets, constitutes an independent source of validation data, hereafter referred to as Indep. The data at all the Indep sites have been partly published [33] and span one calendar year of 1-min observations of GHI, DIF and DNI. With respect to the original dataset used in [28], one station (Cal Poly Humboldt, in the United States) is excluded here because too many observations were flagged during the quality control process.

The Train, Valid and Indep datasets spread across all continents and all primary Köppen–Geiger (KG) climates (namely, Tropical, or type A, with 10 Valid and Train stations and 9 Indep stations; Arid, or type B, with 10 Valid and Train stations and 21 Indep stations; Temperate, or type C, with 16 Valid and Train stations and 26 Indep stations; Continental, or type D, with 8 Valid and Train stations and 9 Indep stations; and Polar, or type E, with 8 Valid and Train stations and no Indep stations). After quality control [28,29], a total of ≈40 million data points with solar zenith angle below 85° remain in the Train dataset, ≈10 million in the Valid dataset, and 14 million in the Indep dataset. The spatial distribution of the stations in the two databases is shown in Fig. 2 of Ruiz-Arias and Gueymard [28].

3. Methodology

The evaluation of all ANN and benchmark models is based on conventional error metrics, such as mean bias error (MBE) and root mean square error (RMSE) [34], calculated from measurements at all observation stations (Section 3) and stratified by sky conditions. A performance ranking is also provided following the methodology used in a previous benchmark analysis [19], to which the interested reader is referred for further details.

3.1. ANN models

The GHI separation is intentionally performed with a basic multilayer feedforward ANN model [35,36]. Although more advanced ANNs might produce better results [37–40], that would be at the cost of increased complexity and reduced universality, as discussed in Section 1.

A multilayer feedforward ANN processes its input unidirectionally across various data processing layers. The input layer has one neuron for each ANN input feature. The subsequent layers, customarily known as hidden layers, transform and transfer their inputs to the following layers. The last is the output layer, which returns the response of the model. In this study, the neural architecture, which is implemented in Python using the Tensorflow framework, is composed of an input layer, two hidden layers of 64 and 32 neurons, respectively, and an output layer. The mean square error is used as both the loss function and the target metric in a conventional randomized cross-validation to evaluate the optimal ANN hyperparameters. The training is carried out for 30 epochs using a batch size of 256 samples and the Adam optimizer with a learning rate of 0.001.

With that methodology, three versions of the ANN model are trained using the Train dataset (Section 2). The first model, hereafter referred to as N1, requires the primary KG climate class [41], solar zenith angle at the prediction time, and the 1-min clearness index, K_T, within the preceding 30-min time window, where K_T is, conventionally, GHI normalized by its extraterrestrial solar irradiance counterpart. Specifically, the K_T input vector of 30 values conveys information on the short-term variability of GHI, which is critically important to improve the separation accuracy, as demonstrated by GISPLIT [19]. (A range of window lengths, from 10 to 60 min, was considered in a set of preliminary tests, which indicated that the 30-min window provided the best results in terms of performance and feasibility.) The second ANN model, referred to as N2, is a climate-independent version of N1, in the sense that it does not require the local KG climate class. The last model, referred to as N3, is similar to N2 but adds the clear-sky index (defined as the ratio between GHI and its estimated clear-sky GHI counterpart) as an additional input. The clear-sky solar irradiance is evaluated with the SPARTA model [42] as described in Ruiz-Arias and Gueymard [28].

3.2. Benchmark models

All separation models considered here provide predictions of the diffuse fraction, K = DIF/GHI. From K, DNI is simply obtained from the fundamental closure equation: DNI = (GHI – DIF)/cos$Z$, or DNI = $(1 - K)$GHI/cos$Z$, where Z is the solar zenith angle [43].

The present analysis assesses the performance of the three ANN separation models described above against a robust benchmark constituted of the 13 high-performance models that were already evaluated in Ruiz-Arias and Gueymard [19]. These 13 models have been described

in detail in previous publications, and their inputs are summarized in Table 2 of Ruiz-Arias and Gueymard [19]. For conciseness, they are just succinctly cited here in chronological order of publication (indicated within brackets, just after the model abbreviation used hereinafter), using the conventional small-cap notation to indicate the first author: Perez2 (P2, 2002) [44], Engerer2 (E2, 2015) [16], Paulescu1 (P1, 2019) [45], Abreu (AB, 2019) [46], Starke3 (S3, 2021) [47], Yang4 (Y4, 2022) [18], Paulescu2 (M1, 2023) [Eq (6) in48], Paulescu3 (M2, 2023) [Eq (5) in48], Yang5 (Y5, 2024) [27] and GISPLIT1 (G1), GISPLIT2 (G2), GISPLIT3 (G3) and GISPLIT4 (G4, 2024) [28].

Perez2, which is sometimes also referred to as DIRINDEX, is the only model of this benchmark to have been developed from hourly irradiance data; it is included here because it was considered for a long time the best separation model until the results in Gueymard and Ruiz-Arias [10] were published, where Engerer2 was found to be the best. The original fitting coefficients of Engerer2 (obtained exclusively from Australian data) were later updated to reflect a more global coverage [49].

4. Results

A first overview of the actual performance of the three ANN models, N1, N2 and N3, can be inferred from Fig. 1, which displays the predictions of the three ANN models for all Valid sites combined. All three provide very similar data distributions in the K_T–K space (Fig. 1a–c). N1, which is stratified by primary KG climate, appears to provide a slightly better coverage of the observed K_T–K distribution (underlying gray tones) than the KG-independent N2. However, it does not appear clearly superior to N3, which is KG-independent like N2 but adds clear-sky global irradiance as an additional predictor. This result suggests that the additional information provided by the predictions of a high-performance clear-sky radiation model provides similar benefits to those from climate stratification. As an expected consequence, the use of clear-sky global irradiance as a predictor in N3 also leads to slightly better predictions under cloudless situations.

To visually assess the relative performance of the ANN models against the benchmark models, Fig. 2 compares N3 to the two best conventional (non-ML) models according to previous benchmark studies, Yang5 [27] and GISPLIT1 [19]. N3 sweeps a wider range of observed K_T–K values than the two conventional models. It also provides a generally better fit of the modeled DNI to observations, as shown, for instance, in the case of cloudless DNI (values above ≈800 W/m^2 in Fig. 2d) with Yang5.

4.1. Overall error metrics

Tables 1–4 show the MBE and RMSE metrics of the ANN and benchmark models at all Valid sites combined and at all Indep sites combined, all also stratified by KG primary climate. Note that polar sites (KG type E) are excluded from the average in column AD to make this column truly comparable between the Valid and Indep datasets (the latter dataset does not have any polar site, whereas the former includes eight of them). No clear best model is found in terms of MBE, but N3 is clearly the best performing model in terms of RMSE for both DNI and DIF, for the Valid and Indep datasets, and for all KG climates. The N3 RMSE results for climates A–D combined are consistent between the Valid and Indep sites for both DNI (≈14%) and DIF (≈24%). N3 improves the best conventional model for DNI (G2, 16.5% and 16.9% in theValid and Indep datasets, respectively) and DIF (G2, 28.4%, and G1, 29.9%, in the Valid and Indep datasets, respectively). Note that G3 and G4 cannot be considered truly conventional separation models because they both make use of XGB to separate GHI under highly variable sky situations. At arid sites, N3 yields the smallest RMSE for DNI and the highest for DIF. This is just an artifact of the normalization approach, since the mean observed DNI (DIF) is greater (smaller) at arid sites than at those in other climate zones.

4.2. Site error metrics

Fig. 3 shows the sitewise mean bias error (sMBE) and sitewise root mean-square error (sRMSE) values for all models and all sites in climates A–D (making the Valid and Indep datasets truly comparable). The trend in both sMBE and sRMSE clearly reveals a performance improvement from the oldest model (Perez2, leftmost boxplots) to the newest ANN models (N1–N3, rightmost boxplots). As discussed above, N3 is clearly the best overall performer. It is also remarkable that neither N1 or N2, which produce very similar results to each other, are clearly better than any of the four GISPLIT model versions. This indicates that the specific clear-sky information ingested by N3 (but not by N1 or N2) is highly relevant, even when using ML techniques. Fig. 3 also shows that, prior to Yang5, all models typically produced sitewise irradiance estimates with nonnegligible positive bias for DNI and negative bias for DIF. That was likely caused by a combination of two factors: (i) locality, because such models were traditionally trained with data from very few locations, and (ii) stiffness, because they were based on too simplistic functional forms. As a result, these older models are generally less robust than Yang5 and the more recent models, as shown by the number of outliers beyond the plot limits in Fig. 3b and d. In fact, the only models without outliers beyond these limits are the four GISPLIT versions and N3. This finding indicates greater robustness in these five models than in all 11 others.

Fig. 4 shows the individual sMBE and sRMSE values for both DNI and DIF considering all models and sites, which confirm the results found in Fig. 3 and, in particular, the remarkable improvements achieved by GISPLIT and the ANN-based models. In addition to Alert (ALE), a polar station where irradiance measurements can be affected by errors [50,51], some sites appear particularly challenging for all models, such as FUU (Fukuoka, Japan) and, even more so, CHB (Chiba, Japan). These two locations are characterized by an unusual low fraction of cloudless days and by high solar radiation variability induced by very unstable cloudiness. However, the bias at CHB is so large and consistent (beyond ≈20% for DNI and ≈ −20% for DIF, for all models) that it might alternatively suggest undetected issues with the radiometers. Other locations, such as ADR (Adrar, Algeria) and XIA (Xianghe, China), also challenge the models, but this is likely because their specific aerosol regimes are widely different from those at most other sites, which directly affects the magnitude of the clear-sky DNI and DIF. A similar issue is apparent at SHA (Shagaya, Kuwait) and SOV (Solar Village, Saudi Arabia) because N1 and N2 provide biased estimates of both DIF and DNI (see Fig. 4), whereas N3 is unbiased, or only slightly biased, precisely because it benefits from the additional information brought by the clear-sky index.

4.3. Error metrics by sky type

Fig. 3 indicates that, in general, the sMBE is positive and negative for DNI and DIF, respectively, with all models older than Yang5, except Abreu. The reason is revealed in Fig. 5 as an inability of those models to correctly predict the diffuse fraction under scattered clouds and cloud enhancements [29], when the short-term variability of solar radiation is highest. This confirms the importance of considering an appropriate measure of temporal variability as a model input. Fig. 5 suggests that every model has a specific response signature to sky conditions. For instance, Paulescu1 overestimates (underestimates) DNI (DIF) under all sky conditions, Abreu strongly underestimates (overestimates) DNI (DIF) under cloudless skies, whereas Yang4 yields unbiased, or nearly unbiased, results for overcast, thick and thin clouds, as well as cloud enhancements. Overall, only the four GISPLIT versions and the three ANN models are capable of providing unbiased or nearly unbiased results for all six sky conditions. This could be expected with GISPLIT because it was specifically developed as a metamodel made up of six submodels, one for each of these sky conditions. The three ANN models

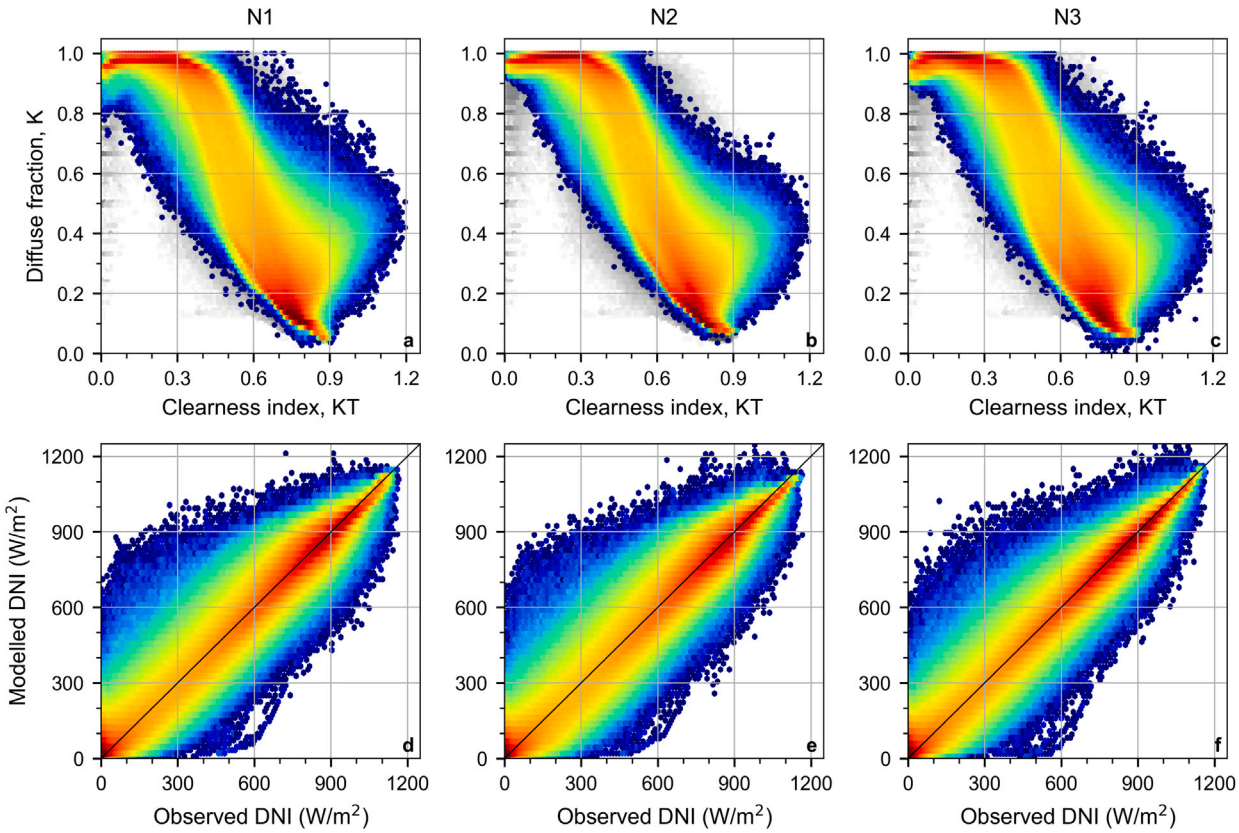

Fig. 1. Comparison of modeled and observed solar radiation components at all the VALID sites combined, except those with primary KG climate E, using models N1 (leftmost column), N2 (central column) and N3 (rightmost column). (a–c) Observed K_T *vs.* observed K (gray) and modeled K (color). (d–f) Observed DNI *vs.* modeled DNI.

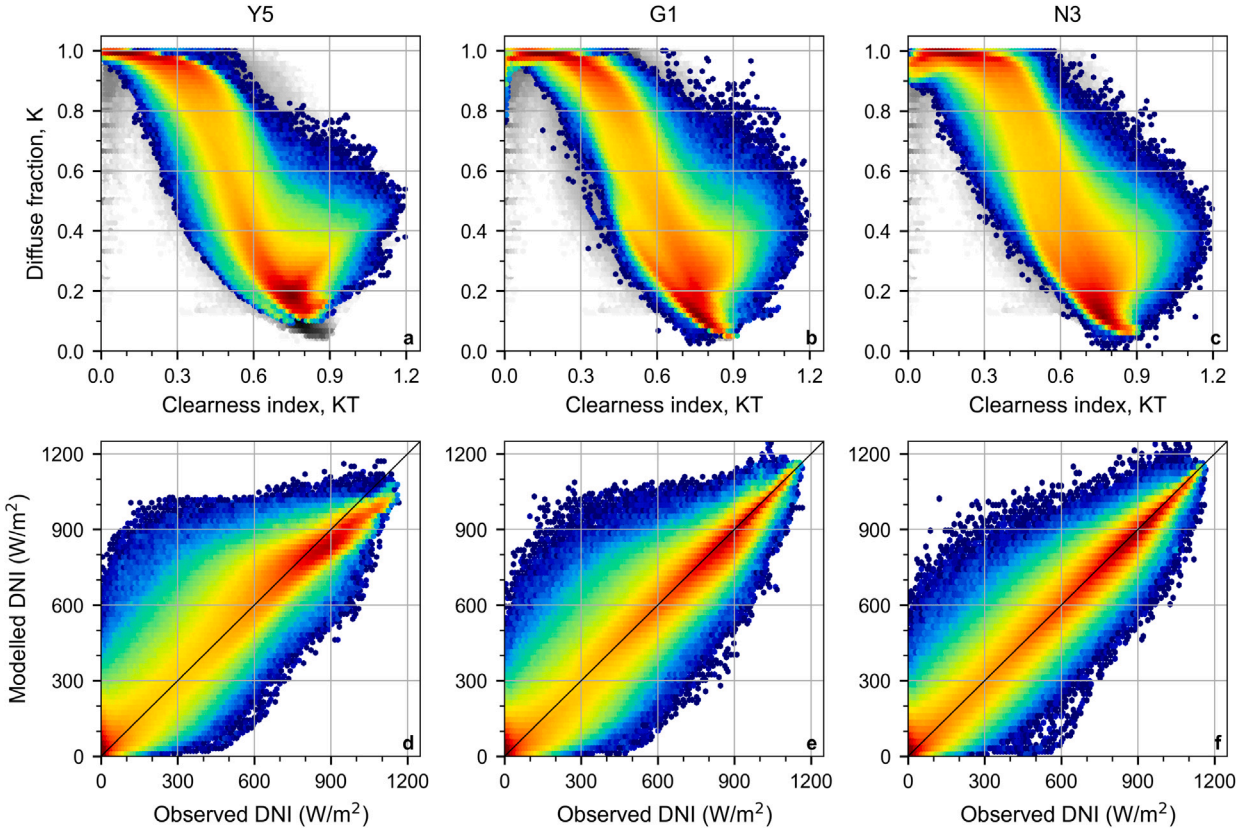

Fig. 2. As Fig. 1 but for models YANG5, GISPLIT1 and N3.

Table 1
DNI MBE and RMSE metrics for the VALID dataset and all separation models. The results are stratified by climate (the column labeled AD combines climates A to D), and are relative to the mean observed DNI, in percent. The lowest error value for each climate is bold-faced.

	MBE (%)						RMSE (%)					
	A-D	A	B	C	D	E	A-D	A	B	C	D	E
P2	6.4	13.2	−2.0	6.3	7.9	17.4	22.9	29.9	13.8	22.3	26.4	48.3
E2	3.4	5.4	−2.2	3.0	8.6	17.0	24.3	27.4	16.4	24.4	30.4	41.1
PB	6.2	5.3	7.1	4.1	11.2	18.2	24.3	26.3	17.8	23.4	32.0	45.2
AB	−2.9	−0.5	−8.1	−3.3	1.3	7.6	26.1	27.8	19.8	26.6	30.7	42.7
S3	3.0	0.3	3.5	2.2	7.8	19.5	19.9	22.3	13.9	19.4	25.7	41.9
Y4	1.2	1.6	−1.0	0.6	5.1	11.7	20.2	22.5	13.8	20.1	25.6	37.1
M1	3.1	−0.7	5.4	2.0	8.1	21.7	19.7	21.5	14.4	18.9	25.9	44.0
M2	3.2	3.2	2.5	1.7	7.4	15.9	22.4	24.9	15.5	22.0	28.9	42.5
Y5	1.8	2.4	−1.8	1.7	5.8	2.7	19.8	21.9	13.7	19.8	24.8	31.1
G1	−0.1	0.4	−2.7	0.4	1.3	7.6	16.9	19.6	11.2	16.9	20.5	28.6
G2	0.1	0.7	0.4	**−0.3**	−0.4	0.4	16.5	19.2	10.4	16.7	20.1	25.5
G3	**−0.0**	**0.0**	−2.2	0.7	1.2	4.6	16.0	18.5	10.5	16.1	19.5	26.4
G4	0.0	0.7	0.4	−0.3	−0.5	0.4	15.7	18.2	9.8	16.0	19.1	24.3
N1	0.9	2.5	**−0.0**	0.7	**0.2**	**−0.4**	15.8	17.5	10.9	15.8	19.5	26.3
N2	−0.3	−2.3	−0.6	−0.3	2.7	8.5	16.2	18.9	11.2	15.9	19.7	30.4
N3	0.1	0.4	−2.0	0.6	1.7	3.9	**14.1**	**16.3**	**9.1**	**14.1**	**17.3**	**23.7**

Table 2
As Table 1 but for the INDEP dataset.

	MBE (%)						RMSE (%)					
	A-D	A	B	C	D	E	A-D	A	B	C	D	E
P2	8.5	18.2	4.6	8.6	8.2	–	23.4	34.9	15.9	25.2	25.2	–
E2	2.4	7.2	**0.3**	2.1	4.0	–	23.4	27.2	18.1	25.5	26.9	–
PB	9.1	6.1	12.5	6.8	10.4	–	24.2	24.5	21.9	24.4	29.4	–
AB	−3.8	**0.1**	−5.3	−4.0	−3.4	–	25.5	27.5	20.4	27.7	30.0	–
S3	4.1	2.0	6.9	1.8	6.4	–	19.8	21.7	17.1	20.4	23.4	–
Y4	0.6	3.8	0.7	−0.3	**−0.1**	–	19.0	22.6	14.9	20.2	22.4	–
M1	4.6	1.2	7.8	2.3	7.4	–	19.2	20.0	16.7	19.6	24.1	–
M2	4.6	4.4	6.1	3.0	5.9	–	21.6	23.8	18.0	22.4	26.3	–
Y5	1.3	2.2	1.5	0.6	1.8	–	18.5	20.6	14.5	19.8	22.6	–
G1	2.0	4.2	1.6	1.8	1.6	–	16.9	20.2	12.5	18.7	19.6	–
G2	2.0	2.9	3.6	0.2	2.2	–	16.9	19.1	12.8	18.8	19.7	–
G3	1.9	2.7	1.8	1.8	2.0	–	16.2	18.7	12.1	18.0	18.8	–
G4	1.8	2.9	3.6	**0.0**	1.7	–	16.4	18.2	12.4	18.3	19.0	–
N1	**0.5**	4.2	1.8	−0.6	−2.7	–	15.9	18.0	13.0	16.9	18.2	–
N2	−0.6	−1.9	1.1	−1.4	−1.0	–	16.2	19.0	12.8	17.6	17.8	–
N3	1.8	2.2	1.4	1.9	2.1	–	**14.0**	**16.1**	**10.5**	**15.5**	**16.2**	–

Table 3
As Table 1 but for DIF.

	MBE (%)						RMSE (%)					
	A-D	A	B	C	D	E	A-D	A	B	C	D	E
P2	−8.2	−19.2	6.2	−9.2	−9.6	−13.7	40.2	46.3	40.9	38.8	33.9	44.5
E2	−1.6	−5.4	11.0	−2.6	−10.0	−17.0	43.2	39.4	51.1	42.6	39.9	46.9
PB	−13.2	−7.7	−20.2	−10.9	−17.1	−24.6	42.7	36.9	52.7	40.6	42.4	54.4
AB	8.2	0.4	27.1	7.1	−3.2	−1.1	47.5	38.7	62.8	47.6	39.4	55.3
S3	−4.5	1.1	−7.9	−3.5	−10.2	−24.6	34.2	31.2	40.5	32.9	33.0	52.4
Y4	−0.6	−1.2	4.9	−0.6	−6.8	−14.1	36.4	32.9	42.5	36.1	33.7	45.4
M1	−7.4	2.4	−16.3	−6.1	−11.8	−31.7	35.8	31.8	43.9	34.0	35.0	59.2
M2	−6.9	−5.4	−6.5	−5.8	−12.0	−21.1	38.4	34.6	45.4	37.0	37.4	50.4
Y5	0.5	−1.0	9.9	−1.1	−6.2	−1.8	35.8	31.9	43.6	35.5	32.0	36.2
G1	0.9	0.6	6.5	−1.0	−1.7	−8.0	28.9	29.0	31.4	28.8	26.1	32.9
G2	**−0.0**	**−0.2**	**−0.4**	0.2	0.3	0.9	28.4	28.7	30.2	28.4	25.6	28.8
G3	0.6	0.8	5.2	−1.2	−1.4	−4.4	27.4	27.3	29.6	27.3	24.6	29.3
G4	0.0	−0.4	−0.5	0.3	0.5	0.8	26.9	27.1	28.7	27.0	24.2	27.2
N1	−0.6	−3.0	2.5	−1.4	**0.2**	**0.2**	27.6	25.2	32.9	27.2	24.8	31.3
N2	0.5	3.7	1.2	**0.0**	−3.5	−9.3	27.8	27.0	32.1	27.2	24.8	35.3
N3	0.9	0.2	6.4	−0.7	−1.8	−2.8	**24.2**	**23.9**	**26.4**	**24.1**	**21.8**	**27.0**

perform in a similar way without the need for submodeling, which constitutes a significant advantage compared to GISPLIT.

The RMSE results in the lower-row panels of Fig. 5 confirm that both scattered-cloudiness and cloud-enhancement situations are the most challenging cases and that all models struggle with them. Unexpectedly, cloudless skies also appear challenging in general, but PEREZ2, GISPLIT, and N3 clearly provide superior results in that case.

4.4. Error metrics by clearness index

Fig. 6 describes the performance of the separation models in terms of K_T. It reveals that N3 performs best for intermediate K_T values, typically corresponding to highly variable situations, while G3 performs better in the case of cloud enhancements, as also confirmed in Fig. 5.

Table 4
As Table 3 but for the INDEP dataset.

	MBE (%)						RMSE (%)					
	A-D	A	B	C	D	E	A-D	A	B	C	D	E
P2	−12.5	−24.9	−9.0	−11.8	−10.8	–	40.8	50.1	38.2	40.9	37.0	–
E2	−2.2	−8.6	**1.3**	−2.1	−5.0	–	42.8	39.0	45.9	41.8	41.9	–
PB	−19.4	−10.4	−32.7	−12.0	−17.8	–	44.8	34.2	56.2	38.9	45.0	–
AB	6.5	−2.1	12.2	5.2	4.6	–	45.7	37.8	51.2	43.4	46.6	–
S3	−6.6	−2.5	−14.1	−1.0	−9.1	–	34.7	29.4	40.1	31.8	34.7	–
Y4	−1.4	−5.4	−2.2	**0.3**	−0.8	–	34.9	32.8	38.3	33.0	34.8	–
M1	−9.7	**−1.3**	−19.4	−3.4	−12.9	–	35.7	28.0	42.5	31.7	38.2	–
M2	−10.0	−8.2	−15.3	−5.9	−10.8	–	38.7	33.1	44.7	35.3	39.9	–
Y5	−1.0	−2.2	−2.0	0.4	−1.7	–	34.0	30.1	36.9	32.5	35.1	–
G1	−2.9	−4.9	−3.9	−1.6	−2.3	–	29.9	28.5	30.4	30.1	29.6	–
G2	−3.3	−4.3	−8.6	1.1	−2.8	–	30.4	27.8	31.2	30.7	29.8	–
G3	−3.1	−3.9	−4.4	−1.9	−2.5	–	28.8	26.7	29.5	29.2	28.3	–
G4	−3.1	−4.5	−8.2	1.3	−2.1	–	29.5	26.4	30.4	30.0	28.5	–
N1	−0.4	−5.7	−2.3	1.6	3.8	–	28.4	25.5	32.3	26.6	27.0	–
N2	**0.3**	2.2	−3.3	2.5	**0.6**	–	28.5	26.2	31.7	27.4	26.1	–
N3	−2.7	−3.4	−3.2	−2.2	−2.5	–	**24.8**	**23.2**	**25.8**	**24.8**	**24.1**	–

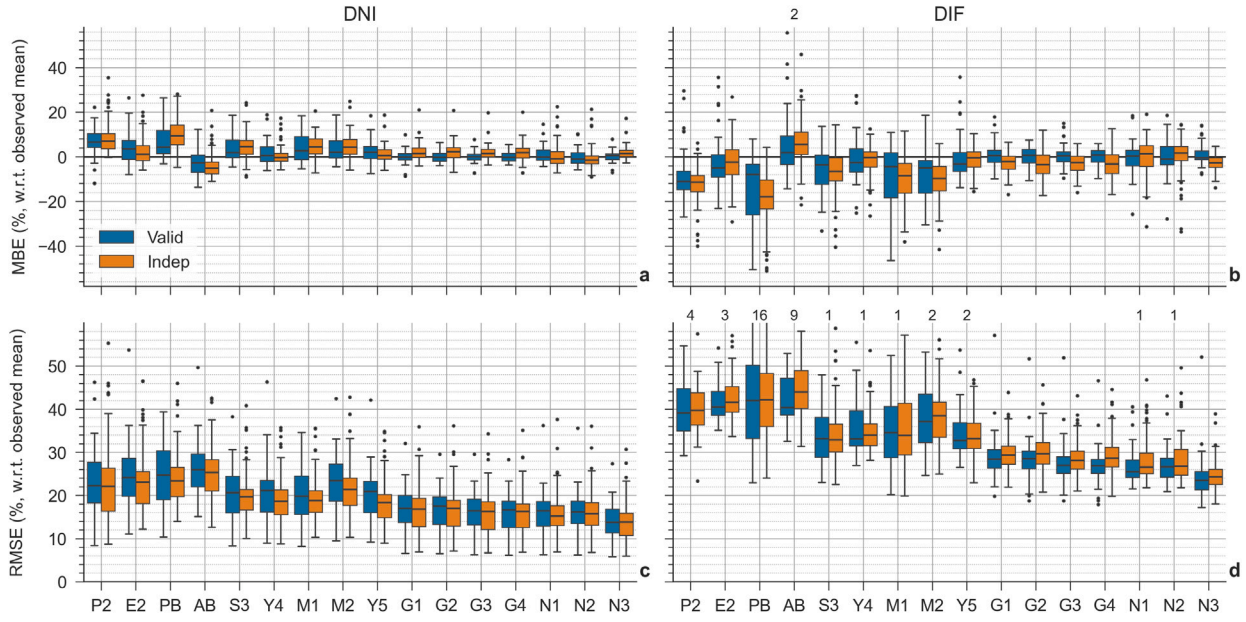

Fig. 3. Sitewise error metrics relative to the mean observed DNI and DIF in each case for all VALID and INDEP sites in climates A–D. (a) MBE for DNI, (b) MBE for DIF, (c) RMSE for DNI and (d) RMSE for DIF. The upper and lower bounds of the boxes extend from the lower to the upper quartiles. The whiskers extend 1.5 times the inter-quartile range from the box. The mean value is indicated with a black horizontal line within the boxes. The figures in the upper side of panels (b) and (d) indicate the number of outliers beyond the plot limits for each model. The models are sorted chronologically by publication date.

This suggests that the discrimination of cloud enhancement situations among highly variable conditions is not as efficient in N3 as in G3.

4.5. Model ranking

For practical purposes, solar analysts need to know which model is best under global or specific conditions, hence model ranking has become an important part of performance analyses for this purpose [10,18,19,27]. Here, like in Ruiz-Arias and Gueymard [19], models are sorted using the sitewise mean linear rank and Diebold–Mariano rank, both evaluated from the daily-mean square errors. The results appear in Table 5 and Fig. 7, revealing that N3 ranks first in all categories. It can thus be referred to as the indisputable best performer relative to this benchmark. Its superiority over N1 and N2 comes from the addition of the estimated clear-sky GHI as a key input. Furthermore, the three ANN models and the four GISPLIT versions rank in the first seven positions for both ranking methods and for both DNI and DIF, although with different orderings. Interestingly, the mean linear ranking reveals a notable numerical gap between ranks 7 and 8.

From these results, it is clear that ANN models and ML can help improve the conventional (non-ML) modeling approaches, because the four top spots are always filled by one or more of them. Nevertheless, using ANN or other ML techniques is not always a guarantee of improvement. For instance, G1 and G2 are better than N2 at predicting DNI and DIF according to the Diebold–Mariano ranking. This is because, in particular, G2 is better than N3 at various stations, such as CAP (Cape Grim, Australia), SBO (Sede Boker, Israel), TAM (Tamanrasset, Algeria), or XIA (Xianghe, China) (Fig. 4). All this suggests that the core GISPLIT modeling approach already represents the state-of-the-art in terms of conventional separation, which the ANN approach can surpass at most sites only if a good estimate of the clear-sky GHI is also used as input.

5. Discussion

This section discusses the variance of the performance of the different models throughout the observational sites, as is graphically evidenced in Fig. 4 and numerically in Tables A.1–A.8. To simplify the

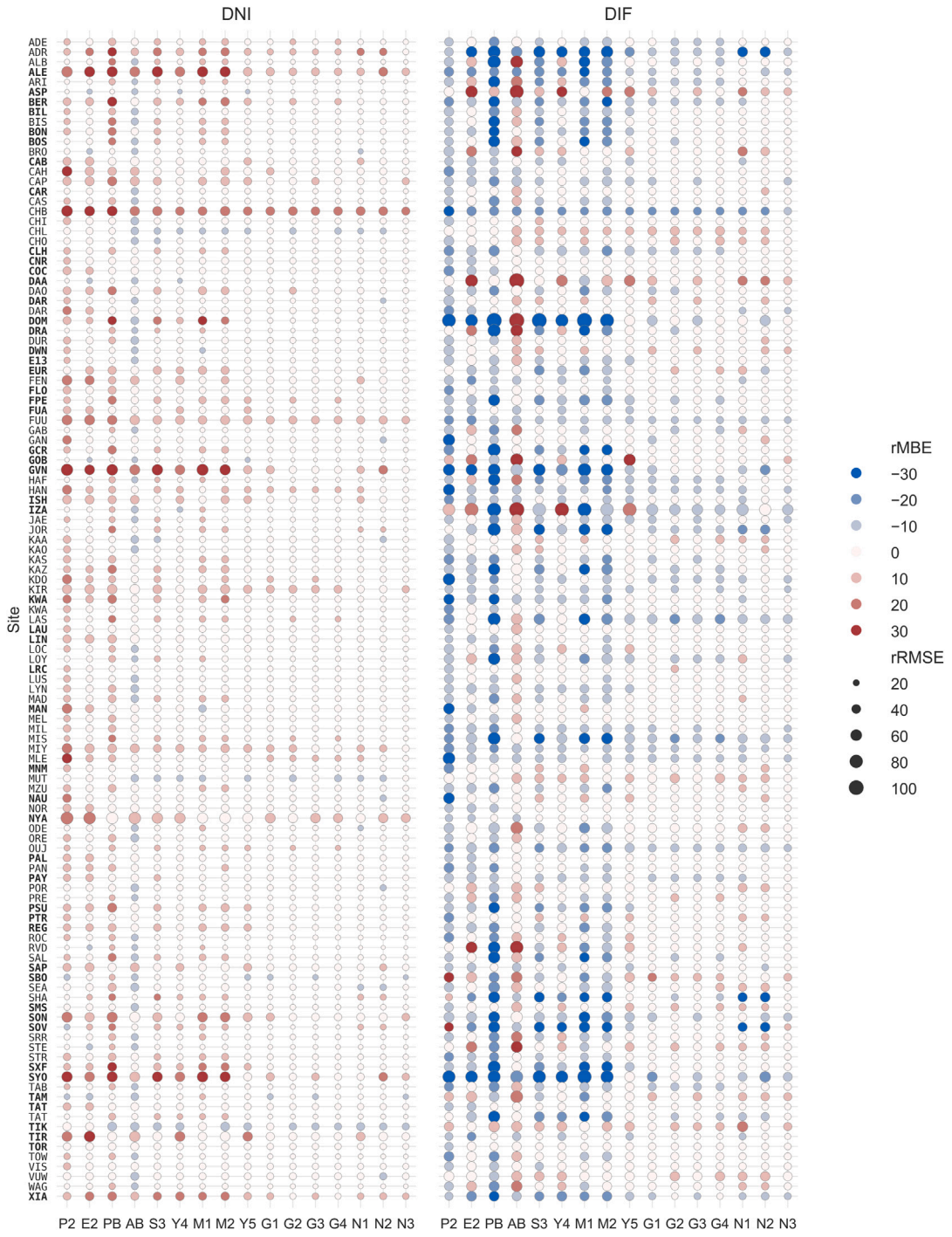

Fig. 4. MBE (marker's color) and RMSE (marker's size) for each site and model. The left panel is for DNI and the right panel is for DIF. The values are in % with respect to the mean DNI at each site (left panel) and the mean DIF at each site (right panel). Note that this explains why the magnitudes of MBE and RMSE are generally higher for DIF than for DNI. (The mean of DNI is normally higher than the mean of DIF.) Sites from the VALID dataset are highlighted in boldface.

analysis, the discussion focuses on the sRMSE metric, which is expected to be low at sites where the radiative climate is only marginally affected by complex cloud situations, under which separation models struggle most (i.e., Sc and Ce sky classes, per Fig. 5). Unsurprisingly, therefore, many dry sunny sites in arid climates (KG class B) end up with a favorable score in Tables A.1–A.8. However, the quality of the measured irradiance at some sites might be an additional factor in explaining why not all stations in class B have low sRMSE.

In general, N3 obtains the best mean DNI sRMSE in each KG class for the VALID and INDEP sites combined (Table 6), generally by a significant margin compared to its closest competitor (typically N1 or G4). Moreover, for KG classes A and E, N3's mean DNI sRMSE is half that of PEREZ2, which is noteworthy. The largest mean sRMSE is for stations with KG class E, which is not surprising because of the specific conditions there: low mean DNI, low sun geometry, significant cloudiness, and harsh conditions that can seriously impact measurement quality [50,51]. The three ANN models, but especially N3, and the GISPLIT family achieve a low standard deviation of sRMSE in each KG class, indicating that they are not too sensitive to climate variability within each KG class. For N3, this standard deviation is less than half that of PEREZ2 on average, for example.

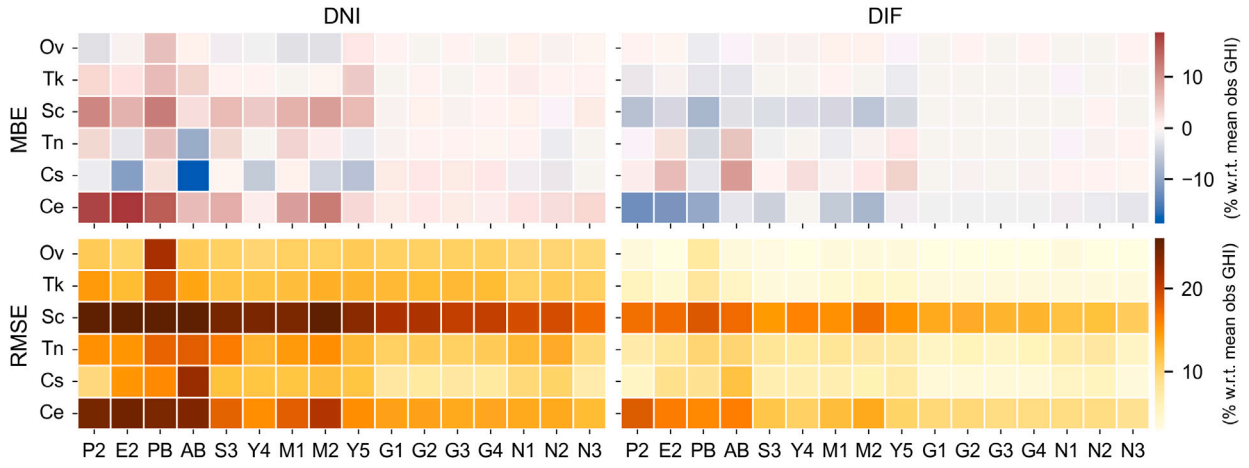

Fig. 5. Error metrics by sky type at all VALID and INDEP sites combined (excluding sites with KG primary climate E). The error is normalized with respect to the mean observed GHI to prevent normalizing by very small DNI under overcast conditions. As defined in [29], the six possible sky types are overcast (Ov), thick clouds (Tk), scatter clouds (Sc), thin clouds (Th), cloudless (Cs) and cloud enhancement (Ce).

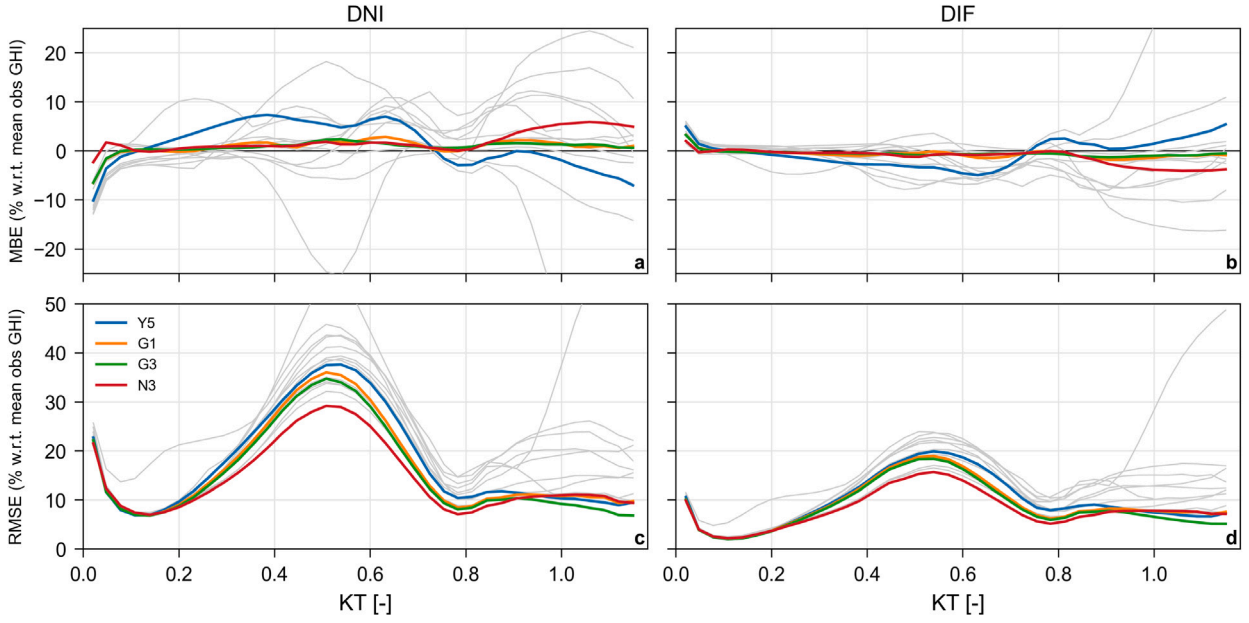

Fig. 6. Error metrics as a function of K_T for all VALID and INDEP sites combined (excluding climate-E sites).

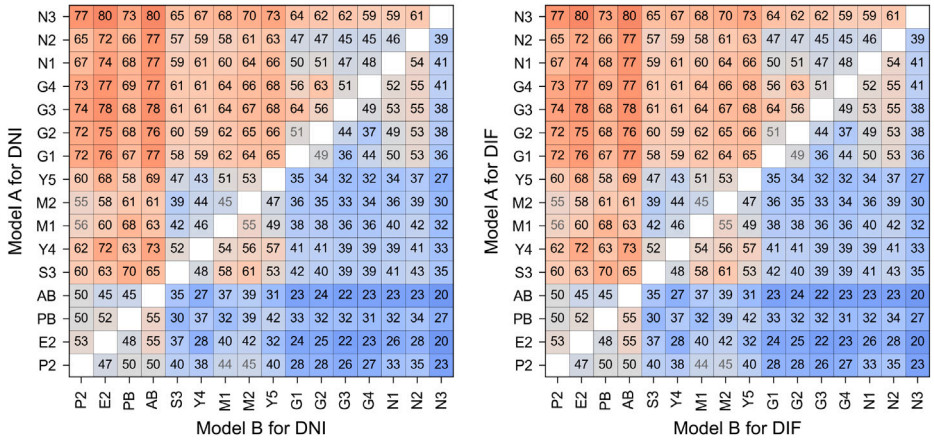

Fig. 7. Pairwise comparison of model predictions for both DNI (left panel) and DIF (right panel). The numbers in the cells represent the percentage of prediction instances for which Model A is better than Model B (e.g., GISPLIT1 is better than STARKE3 for 58% of the DNI prediction instances, and for 58% of the DIF prediction instances). The prediction instances are daily averages for the observational sites of the VALID and INDEP datasets combined. Cells shaded in gray indicate that the corresponding Diebold–Mariano test is not significant.

Table 5
Model ranking based on the mean square error for the combined VALID and the INDEP datasets. The mean linear rank is evaluated from the sitewise mean square errors. The Diebold–Mariano rank uses the daily mean square errors for all sites. For the mean linear rank, the number in parenthesis is the mean rank value of each model. For the Diebold–Mariano test rank, it is the fraction of evaluation days in which the model is better than the following in the rank (e.g., for DNI, G4 is better than G3 for 51% of the days).

Position	Mean linear rank				Diebold–Mariano test rank			
	DNI		DIF		DNI		DIF	
1	N3	(1.2)	N3	(1.2)	N3	(59)	N3	(59)
2	N1	(3.8)	N2	(4.0)	GISPLIT4	(51)	GISPLIT4	(51)
3	GISPLIT4	(3.9)	GISPLIT3	(4.1)	GISPLIT3	(53)	GISPLIT3	(53)
4	GISPLIT3	(4.0)	N1	(4.1)	N1	(51)	N1	(51)
5	N2	(4.5)	GISPLIT4	(4.2)	GISPLIT2	(51)	GISPLIT2	(51)
6	GISPLIT2	(5.9)	GISPLIT2	(6.2)	GISPLIT1	(53)	GISPLIT1	(53)
7	GISPLIT1	(6.2)	GISPLIT1	(6.3)	N2	(59)	N2	(59)
8	YANG5	(8.7)	STARKE3	(9.4)	YANG4	(52)	YANG4	(52)
9	YANG4	(9.6)	YANG5	(9.4)	STARKE3	(53)	STARKE3	(53)
10	PAULESCU3	(10.0)	PAULESCU3	(10.0)	YANG5	(51)	YANG5	(51)
11	STARKE3	(10.8)	YANG4	(10.3)	PAULESCU3	(55)	PAULESCU3	(55)
12	PEREZ2	(12.3)	PAULESCU2	(12.1)	PAULESCU2	(61)	PAULESCU2	(61)
13	PAULESCU2	(12.4)	PEREZ2	(12.6)	PAULESCU1	(52)	PAULESCU1	(52)
14	ENGERER2	(13.7)	ENGERER2	(13.8)	ENGERER2	(53)	ENGERER2	(53)
15	PAULESCU1	(14.2)	PAULESCU1	(13.9)	PEREZ2	(50)	PEREZ2	(50)
16	ABREU	(14.8)	ABREU	(14.5)	ABREU	(–)	ABREU	(–)

Table 6
DNI site sRMSE metrics by climate, and for climates A–D combined (columns A–D), relative to the mean observed DNI, in percent, for the VALID and INDEP datasets combined and all separation models. The number of samples is given in millions (10^6). The lowest value for each climate is bold-faced.

Climate	A-D	A	B	C	D	E	A-D	A	B	C	D	E
# sites	109	19	31	42	17	8	109	19	31	42	17	8
# samples	22.4	3.8	6.5	8.9	3.2	1.3	22.4	3.8	6.5	8.9	3.2	1.3
sRMSE	Mean (%)						Standard deviation (%)					
P2	23.2	32.3	15.3	24.2	25.7	48.3	9.0	8.4	4.6	8.1	5.1	15.3
E2	23.8	27.3	17.6	25.1	28.5	41.1	7.4	7.6	4.0	6.8	5.5	13.5
PB	24.2	25.4	20.7	24.0	30.6	45.2	6.7	6.1	5.5	6.5	5.0	10.4
AB	25.8	27.7	20.3	27.3	30.3	42.7	6.1	6.0	3.4	5.1	4.9	11.5
S3	19.9	22.0	16.2	20.0	24.5	41.9	5.8	4.9	4.8	5.5	4.5	9.7
Y4	19.5	22.6	14.6	20.2	23.9	37.1	6.1	6.7	3.9	5.1	4.6	10.2
M1	19.4	20.8	16.1	19.3	24.9	44.0	5.5	4.6	4.5	5.1	4.5	9.6
M2	21.9	24.4	17.2	22.3	27.5	42.5	6.5	5.9	4.8	6.1	4.5	10.1
Y5	19.0	21.3	14.3	19.8	23.6	31.1	5.6	5.6	3.4	5.1	4.1	9.3
G1	16.9	19.9	12.1	18.0	20.0	28.6	5.3	4.3	3.2	4.9	3.7	9.7
G2	16.7	19.1	12.1	18.0	19.9	25.5	5.2	4.1	3.4	4.9	4.0	8.2
G3	16.1	18.6	11.6	17.3	19.1	26.4	5.0	4.0	3.1	4.8	3.6	9.2
G4	16.1	18.2	11.7	17.4	19.0	24.3	5.1	4.0	3.3	4.9	3.8	7.9
N1	15.9	17.8	12.4	16.5	18.8	26.3	5.1	5.1	3.9	5.1	**2.8**	**7.4**
N2	16.2	18.9	12.3	17.0	18.6	30.4	5.1	4.7	3.9	5.0	3.2	8.4
N3	**14.0**	**16.2**	**10.1**	**15.0**	**16.7**	**23.7**	**4.5**	**3.7**	**2.7**	**4.5**	3.2	8.2

Table 7
As Table 6 but for DIF.

Climate	A-D	A	B	C	D	E	A-D	A	B	C	D	E
# sites	109	19	31	42	17	8	109	19	31	42	17	8
# samples	22.4	3.8	6.5	8.9	3.2	1.3	22.4	3.8	6.5	8.9	3.2	1.3
sRMSE	Mean (%)						Standard deviation (%)					
P2	40.5	48.2	38.9	40.2	35.6	44.5	6.9	8.1	4.9	5.9	3.9	14.7
E2	43.0	39.2	47.4	42.1	41.0	46.9	6.8	1.8	7.1	6.8	5.2	12.9
PB	44.0	35.6	55.2	39.5	43.8	54.4	12.4	7.0	11.0	10.0	10.0	22.7
AB	46.4	38.2	54.5	45.0	43.3	55.3	14.3	3.0	14.1	16.1	7.7	25.3
S3	34.5	30.3	40.2	32.2	33.9	52.4	7.9	3.1	7.3	7.9	6.3	22.4
Y4	35.5	32.8	39.5	34.1	34.3	45.4	7.3	**1.6**	6.5	8.7	5.6	16.0
M1	35.7	29.9	42.9	32.5	36.7	59.2	9.5	4.6	8.1	9.0	8.3	28.6
M2	38.6	33.9	44.9	36.0	38.7	50.4	8.1	4.7	7.0	7.5	7.2	18.6
Y5	34.7	31.0	38.8	33.6	33.6	36.2	7.5	2.8	7.5	8.2	5.3	9.8
G1	29.5	28.7	30.7	29.6	28.0	32.9	4.7	2.9	4.4	5.6	3.8	9.1
G2	29.6	28.2	30.9	29.9	27.9	28.8	4.9	3.0	4.6	5.5	4.3	7.3
G3	28.3	27.0	29.5	28.5	26.6	29.3	4.6	2.6	4.4	**5.2**	3.8	7.2
G4	28.5	26.8	29.9	28.9	26.5	27.2	4.8	2.8	4.5	5.5	4.1	**6.6**
N1	28.1	25.3	32.5	26.8	26.0	31.3	6.0	1.9	6.0	6.1	4.1	9.3
N2	28.3	26.6	31.8	27.3	25.5	35.3	6.2	2.6	6.9	6.5	3.7	11.2
N3	**24.6**	**23.6**	**25.9**	**24.5**	**23.0**	**27.0**	**4.3**	2.4	**3.8**	5.3	**3.0**	7.3

Table 8
Mean and N3 sRMSE values for benchmarking and problematic sites with their respective KG climate classes (except sites with KG class E which have all large sRMSE values).

Reference "safe" sites for benchmarking					Most "problematic" sites				
Code	Station	KG class	sRMSE (%)		Code	Station	KG class	sRMSE (%)	
			Mean	N3				Mean	N3
GOB	Gobabeb (NA)	B	8.6	5.8	MIY	Miyako (JP)	A	30.1	22.3
ASP	Alice Springs (AU)	B	8.9	5.8	KIR	Kiruna (SE)	D	33.1	24.2
RVD	Richtersveld (ZA)	B	9.2	5.9	FUU	Fukue (JP)	C	35.1	27.5
DAA	De Aar (ZA)	B	10.3	6.9	TIR	Tiruvallur (IN)	A	38.1	27.4
DRA	Desert Rock (US)	B	11.2	7.4	CHB	Chiba (JP)	C	39.0	30.7

Table A.1
DNI MBE in percent by site in each climate class, relative to the mean observed DNI, for the VALID dataset and for all separation models. The lowest error for each site is bold-faced.

Site	P2	E2	PB	AB	S3	Y4	M1	M2	Y5	G1	G2	G3	G4	N1	N2	N3
Köppen-Geiger climate A																
BER	13.7	10.6	26.5	3.8	14.0	7.3	16.2	18.8	7.8	4.5	6.4	4.6	5.5	4.7	**2.6**	3.8
COC	14.2	5.3	4.2	0.5	0.2	0.4	−1.7	3.1	**0.1**	−0.1	0.3	0.1	0.8	1.6	−1.7	1.2
DAR	5.0	−2.2	−1.4	−8.0	−4.3	−2.5	−4.5	−2.5	**−0.4**	−2.6	−2.3	−2.8	−2.3	0.5	−5.2	−2.5
DWN	6.0	−1.3	−2.7	−7.3	−4.1	−2.5	−5.4	−3.4	**−0.4**	−2.5	−2.6	−2.8	−2.5	0.9	−4.2	−2.8
ISH	14.5	11.5	7.5	5.1	3.5	6.5	1.7	5.8	6.4	1.3	1.8	**1.0**	1.8	7.0	2.1	1.5
KWA	17.5	8.8	21.0	3.4	9.9	4.9	10.6	15.5	4.3	2.5	3.2	1.7	2.2	4.6	**1.1**	1.1
MAN	22.2	5.4	1.7	0.5	−3.1	**−0.2**	−5.1	0.7	−0.5	4.8	4.2	3.6	3.7	1.1	−4.4	2.5
MNM	10.7	1.3	0.7	−3.0	−1.6	−2.0	−4.4	−0.5	0.7	−1.7	−2.0	−1.2	−1.0	−1.1	−3.9	**−0.4**
NAU	16.0	1.9	2.6	−3.6	−2.8	−2.7	−3.4	1.5	−3.0	0.3	**−0.1**	−0.4	−0.1	−1.8	−5.7	0.5
TIR	16.3	26.4	1.0	12.4	−3.6	17.0	−4.1	−0.4	18.4	**−0.0**	0.1	−3.0	1.1	14.6	−0.8	0.2
Köppen-Geiger climate B																
ASP	−1.3	−8.0	−1.8	−13.0	−2.2	−6.2	−1.0	−4.5	−5.0	−2.6	**−0.9**	−2.4	−0.9	−3.6	−3.7	−2.3
BOS	3.2	−0.5	15.1	−6.9	7.4	−0.8	10.9	7.2	2.3	−1.1	2.7	−0.7	2.2	**0.0**	−1.4	0.1
DAA	−0.7	−7.3	0.7	−13.6	**−0.5**	−5.4	2.1	−2.5	−3.8	−3.1	−0.8	−2.6	−0.5	−4.1	−4.9	−2.0
DRA	**0.6**	−4.3	12.7	−10.2	5.8	−1.6	8.5	3.9	0.6	−1.4	1.5	−1.0	1.2	−1.2	−2.0	−1.1
FPE	6.6	4.4	15.4	−2.8	9.8	4.4	11.2	9.4	5.6	1.6	5.7	1.3	5.1	3.2	1.4	**0.8**
GOB	−2.8	−5.0	2.1	−9.9	1.5	−3.3	1.5	−0.8	−7.5	−1.3	0.4	−1.2	0.5	−0.2	**0.1**	−2.3
PTR	9.6	1.1	**0.1**	−4.6	−4.6	−4.0	−4.5	−0.9	−4.0	−1.4	0.3	−0.6	0.5	−4.3	−4.6	0.3
SBO	−11.9	−3.5	5.4	−8.7	1.0	**−0.6**	4.2	1.4	−5.4	−8.7	−3.6	−7.2	−2.7	−1.1	−1.6	−6.0
SOV	−11.8	7.2	16.2	0.8	13.3	9.6	14.8	11.6	3.6	−3.7	**0.7**	−2.2	0.7	10.4	10.3	−2.8
TAM	−5.9	−5.6	4.2	−11.8	1.9	−3.4	6.1	**−0.2**	−3.2	−8.0	−2.0	−7.4	−2.0	−2.8	−4.8	−7.1
Köppen-Geiger climate C																
BIL	5.2	−1.0	6.9	−6.5	2.2	0.7	3.4	2.4	3.4	−0.8	−1.9	−0.5	−1.7	−1.5	−2.6	**−0.1**
CAB	11.5	9.8	2.4	1.8	4.7	4.8	2.6	**1.7**	7.0	3.3	2.6	3.7	2.4	5.0	3.3	4.4
CAR	2.8	−2.0	−2.9	−8.0	−2.4	−1.6	−3.0	−3.7	1.3	−1.1	−2.0	**−0.9**	−2.1	−2.1	−3.4	−1.2
CLH	10.0	4.2	10.6	**−0.8**	7.6	3.4	5.8	7.5	2.7	3.2	3.0	3.1	2.9	2.0	0.8	1.6
CNR	5.5	3.6	0.7	−2.8	0.4	0.3	0.2	−0.6	1.4	**−0.1**	−0.7	0.3	−0.8	0.6	0.1	0.6
E13	5.2	−0.1	4.8	−6.0	1.8	0.8	2.9	1.8	3.7	−0.3	−1.1	**0.0**	−1.0	−0.5	−1.5	0.0
FLO	10.9	2.7	5.6	−2.5	1.1	−0.4	0.4	2.4	**−0.3**	1.7	0.9	1.6	0.8	−1.6	−2.0	0.9
FUA	7.6	8.6	2.0	2.1	1.5	6.0	**0.2**	0.8	5.9	0.9	−1.7	1.1	−1.7	4.0	3.0	1.2
GCR	6.4	1.6	23.0	−2.7	8.6	2.5	11.6	11.7	1.6	−1.1	−2.2	−1.1	−2.5	−1.5	−2.1	**−0.9**
IZA	−2.9	−3.9	10.0	−12.9	1.9	−5.6	8.6	3.7	−3.7	0.8	1.5	1.1	1.6	1.6	**−0.2**	0.7
LAU	5.0	2.3	2.6	−4.7	1.9	−3.3	2.7	2.3	−1.5	0.7	1.5	0.9	0.7	−1.6	−2.7	**0.5**
LRC	5.3	0.5	1.8	−4.4	0.6	−1.5	−1.1	**−0.2**	−1.6	−2.1	−2.6	−2.1	−2.6	−1.5	−2.3	−2.1
PAL	10.2	7.7	2.3	**0.2**	3.6	2.4	1.7	1.6	4.0	2.2	1.5	2.5	1.4	3.6	2.6	3.0
PAY	10.3	5.6	4.7	**−0.3**	5.0	3.3	3.7	3.2	3.9	4.2	4.0	4.6	3.9	4.2	2.7	3.9
SMS	2.4	−2.5	1.5	−8.1	−1.7	−4.3	**−1.2**	−1.7	−4.1	−3.3	−3.9	−2.8	−3.7	−4.2	−4.4	−2.5
TAT	5.6	7.0	0.7	0.9	1.6	2.6	−1.3	**0.0**	3.2	−1.4	−3.1	−1.3	−3.1	3.0	2.0	−1.6

(*continued on next page*)

A relatively similar situation is depicted in Table 7 for the corresponding DIF results, with even a much larger improvement for N3 in KG class E. However, climate classes B and E are where the mean DIF sRMSE is maximum and minimum, respectively, thus mirroring the results for DNI discussed just above.

The remarkable spread in station-wise results observed in Tables A.1–A.8 is somehow inherent to separation models because of their simplicity and sensitivity to complex cloudiness situations. It is encouraging, though, that the station-wise sRMSE spread, measured by its standard deviation, tends to decrease in newer, more effective models.

From another perspective, it is desirable to identify stations at the two extremes of the performance range, i.e., with either outstanding or poor separation performance. This information can prove highly useful when developing more in-depth assessments of the performance of various types of radiation models, including (but not limited to) separation models. Table 8 shows the top-5 "safest" and "most problematic" sites within the whole 117-site database, according to the model-wise mean sRMSE criterion applied to DNI.

At the five safest sites (all in climate class B), the N3 sRMSE remains low and ≈30% less than the mean of all models. It is highly likely that these stations record high-quality irradiance time series, since all except RVD belong to BSRN (Section 2), and any decent radiation model should be expected to perform well there. In contrast, the five most problematic sites are affected by high sRMSE, about four times larger than those of the safest sites. None of these sites are in KG Class B, while 3 belong to the Skynet network in Japan (see Table 2

Table A.1 (*continued*).

Site	P2	E2	PB	AB	S3	Y4	M1	M2	Y5	G1	G2	G3	G4	N1	N2	N3
Köppen-Geiger climate D																
BON	7.1	3.8	16.4	−1.8	8.6	3.6	10.5	9.6	4.1	0.4	−1.0	0.5	−1.0	−2.8	**0.2**	0.5
LIN	9.5	9.1	8.3	1.4	4.9	1.6	3.8	4.3	4.4	**−0.2**	−1.4	0.3	−0.9	−0.4	1.4	1.6
PSU	8.7	7.6	22.6	1.4	10.8	4.8	13.8	14.4	5.9	**−0.0**	−1.3	−0.0	−1.6	−0.8	1.4	0.6
REG	6.9	7.0	11.6	**−0.1**	9.5	2.9	10.4	8.9	5.2	2.2	2.7	1.6	1.7	0.4	2.7	1.4
SAP	6.8	11.9	2.3	5.0	3.6	6.3	2.6	2.3	8.2	**−0.3**	−3.0	0.4	−2.5	2.4	5.4	1.4
SXF	6.6	5.5	26.0	**0.1**	13.9	6.7	17.4	15.7	7.4	1.4	−0.4	1.0	−0.9	−1.4	1.7	1.2
TOR	4.6	3.4	−3.1	−4.0	**−0.3**	−1.2	−1.9	−3.7	1.0	−1.7	−2.6	−1.5	−2.5	−2.8	−1.3	−0.6
XIA	14.4	19.5	20.8	8.8	18.6	18.9	18.3	17.4	12.2	9.8	4.5	7.7	**4.4**	6.2	10.0	7.9
Köppen-Geiger climate E																
ALE	22.6	27.3	28.1	20.8	29.9	20.1	30.4	27.8	9.5	13.9	5.8	10.6	**5.0**	5.3	17.0	8.8
DOM	14.0	10.7	27.8	−7.5	20.1	11.0	31.0	20.2	2.2	4.2	−0.1	3.0	0.6	1.6	3.6	**−0.0**
EUR	4.2	9.9	7.0	1.9	13.9	6.8	11.4	7.7	−1.0	1.7	−3.8	0.6	−3.6	−2.7	4.4	**0.5**
GVN	32.4	26.4	36.3	16.4	36.2	22.2	41.2	32.0	8.1	12.2	1.3	4.0	**−0.0**	5.4	17.3	3.8
NYA	22.5	20.7	**0.6**	14.0	11.0	7.7	3.9	1.1	−2.0	12.3	4.9	10.3	6.1	−3.3	7.0	9.2
SON	15.3	11.5	24.4	1.7	13.5	4.8	22.8	18.7	7.8	5.3	−1.8	3.5	**−0.8**	−4.5	4.0	5.4
SYO	25.8	21.6	28.1	13.3	30.8	22.4	35.9	25.6	3.3	11.1	0.7	5.6	**−0.3**	4.3	15.5	6.2
TIK	−2.7	**1.2**	−8.6	−7.4	−5.8	−6.6	−3.1	−9.9	−9.1	−5.0	−8.7	−6.8	−8.6	−13.7	−5.2	−8.6

Table A.2
Same as Table A.1 but for RMSE.

Site	P2	E2	PB	AB	S3	Y4	M1	M2	Y5	G1	G2	G3	G4	N1	N2	N3
Köppen-Geiger climate A																
BER	27.8	30.0	39.4	29.6	27.2	24.2	27.6	33.1	24.2	20.3	20.6	19.2	19.7	17.9	18.4	**16.9**
COC	29.3	26.3	23.2	26.1	20.6	20.9	19.7	22.1	20.7	18.9	18.8	18.0	17.9	16.7	17.6	**15.9**
DAR	20.2	18.4	16.3	21.8	15.0	15.1	13.8	16.1	14.2	13.6	12.9	12.9	12.1	11.6	14.3	**11.2**
DWN	20.6	18.4	17.0	21.7	15.6	15.3	15.1	16.8	14.6	13.8	13.3	13.1	12.6	11.9	14.0	**11.1**
ISH	34.4	35.7	30.3	34.4	25.9	27.5	24.6	30.0	27.0	23.3	23.5	22.4	22.5	22.9	23.1	**19.8**
KWA	31.2	27.2	34.0	26.5	25.2	23.4	24.5	29.4	23.0	19.9	19.7	18.6	18.7	17.3	17.7	**16.9**
MAN	42.4	31.2	30.4	31.1	26.2	26.4	25.9	28.8	25.8	24.8	24.0	23.0	22.6	**19.8**	22.1	20.1
MNM	23.5	22.4	21.2	23.0	18.1	17.6	18.4	19.9	17.7	16.2	16.6	15.5	15.7	14.7	16.1	**13.7**
NAU	33.3	25.1	25.4	25.9	23.0	22.1	21.5	23.9	21.5	20.4	19.5	19.1	18.6	**16.3**	19.1	16.9
TIR	46.2	53.7	38.0	49.7	38.2	46.3	34.6	42.5	42.1	32.1	29.6	29.5	28.3	36.2	35.6	**27.4**
Köppen-Geiger climate B																
ASP	8.4	12.8	10.4	17.8	8.4	9.9	8.2	10.0	9.2	7.3	6.7	6.8	6.4	7.2	7.2	**5.8**
BOS	14.9	18.3	24.5	21.5	17.1	15.1	19.0	19.2	15.0	13.3	13.1	12.7	12.6	11.5	11.6	**10.5**
DAA	9.2	14.3	11.9	20.2	9.1	11.1	9.5	11.7	10.5	8.7	8.1	8.2	7.7	8.6	9.2	**6.9**
DRA	10.4	13.6	18.5	17.7	12.4	10.6	13.7	13.5	10.8	9.1	8.6	8.5	8.2	8.0	8.4	**7.4**
FPE	21.9	23.9	31.0	25.9	24.1	21.3	25.2	26.9	22.1	16.4	18.6	15.8	17.7	16.8	15.8	**13.7**
GOB	8.8	11.1	10.5	15.2	8.4	9.0	8.4	9.5	12.0	6.6	6.5	6.3	6.2	6.3	6.3	**5.8**
PTR	23.9	22.8	21.4	25.2	18.6	18.5	17.6	20.5	17.9	17.0	16.8	16.2	15.8	16.5	15.7	**13.4**
SBO	17.6	18.6	16.8	21.3	14.4	15.9	14.4	16.0	16.3	15.6	11.6	13.9	**10.5**	12.0	13.0	11.7
SOV	16.2	17.2	22.4	17.6	19.2	17.4	19.6	18.9	13.6	11.1	9.2	9.9	**8.6**	15.7	16.4	9.4
TAM	15.2	20.6	16.9	25.9	14.0	16.7	15.8	15.9	16.1	16.2	11.8	15.9	**11.6**	13.0	14.0	13.4
Köppen-Geiger climate C																
BIL	18.4	19.9	22.8	22.5	16.4	15.8	16.4	19.4	15.9	13.3	13.4	12.7	12.9	12.7	13.1	**11.1**
CAB	30.1	33.4	28.0	33.9	25.3	26.3	23.7	27.6	26.2	22.3	21.8	21.6	21.1	21.2	21.2	**19.3**
CAR	16.7	20.4	19.0	24.2	16.0	16.2	15.2	18.9	15.8	13.7	13.8	13.1	13.3	13.6	14.0	**11.6**
CLH	21.0	20.7	22.5	20.9	18.5	18.6	17.5	20.6	18.5	14.9	14.4	14.1	13.9	13.5	13.3	**12.3**
CNR	21.9	27.2	23.5	29.4	20.6	21.6	19.9	23.5	21.2	18.7	18.6	18.0	17.9	16.6	16.7	**15.0**
E13	17.9	19.7	19.0	22.3	15.3	16.2	14.8	18.0	16.3	13.0	13.0	12.5	12.6	12.5	12.8	**11.2**
FLO	27.8	27.8	29.2	29.5	22.0	22.6	22.4	25.8	22.7	19.9	19.7	18.8	18.6	17.1	17.3	**15.5**
FUA	26.2	28.5	25.3	28.1	23.1	24.8	22.1	26.3	23.3	18.9	18.2	17.9	17.4	20.0	19.5	**16.0**
GCR	20.8	20.5	31.6	21.0	18.0	16.6	19.7	22.9	16.2	14.4	14.4	13.8	14.0	13.2	13.5	**11.4**
IZA	12.5	14.0	16.0	22.3	14.2	15.4	14.1	13.2	14.4	10.7	9.6	9.6	**8.4**	11.1	11.3	9.5
LAU	22.6	25.6	27.5	30.2	21.2	22.1	21.6	25.1	22.0	19.2	19.0	18.2	17.9	16.1	16.2	**14.9**
LRC	19.5	19.9	17.9	22.1	15.3	16.1	14.8	16.9	16.1	14.3	14.2	13.7	13.7	13.1	13.4	**12.5**
PAL	27.3	29.7	25.7	31.0	23.1	23.2	21.4	24.9	22.9	20.5	20.3	19.8	19.5	19.2	19.1	**17.2**
PAY	24.3	26.6	24.1	27.6	20.0	21.3	19.3	23.4	21.6	18.6	18.6	18.0	17.8	17.3	16.7	**15.8**
SMS	19.0	22.1	20.0	26.5	16.3	17.5	16.1	19.1	17.8	15.4	15.5	14.6	14.9	14.0	14.5	**13.0**
TAT	27.1	28.8	24.9	29.1	21.3	23.5	21.0	24.2	22.5	19.3	19.0	18.4	18.4	18.5	18.5	**16.4**

(*continued on next page*)

in Ruiz-Arias and Gueymard [28]). Although a particular cloud regime might be impairing better performance there, it is also quite likely that their measurement quality is impacted by more-or-less severe inconsistencies that current QC protocols are not able to flag. This finding should prompt the stations' principal investigators to reevaluate their equipment and maintenance procedures, and the solar radiation modelers to develop more effective modeling strategies and better QC algorithms.

Table A.2 (*continued*).

Site	P2	E2	PB	AB	S3	Y4	M1	M2	Y5	G1	G2	G3	G4	N1	N2	N3
Köppen-Geiger climate D																
BON	21.9	24.0	30.0	25.9	21.0	19.7	21.7	24.8	19.6	16.1	15.9	15.4	15.3	16.4	15.8	**13.7**
LIN	30.5	35.2	33.2	36.2	26.1	26.8	25.0	30.0	26.8	24.0	24.1	23.4	23.3	22.1	21.9	**20.8**
PSU	26.0	29.5	37.7	30.0	24.2	23.5	26.0	31.0	23.3	20.0	20.0	19.3	19.4	18.0	17.7	**16.1**
REG	25.3	26.9	29.1	27.9	26.0	24.0	27.4	27.2	25.1	18.5	18.7	17.4	17.2	19.0	18.6	**15.4**
SAP	29.7	36.3	31.3	35.1	27.9	29.2	27.5	31.4	28.9	23.7	24.0	22.5	22.6	21.8	22.3	**19.5**
SXF	21.5	24.2	36.8	24.9	25.2	21.6	27.7	29.0	21.9	17.0	17.0	16.6	16.4	16.4	16.1	**13.9**
TOR	25.3	28.6	27.3	31.6	23.6	23.2	22.7	26.5	23.3	20.1	19.9	19.4	19.2	19.7	19.4	**16.8**
XIA	27.6	34.5	35.2	29.7	30.7	34.1	29.9	32.1	26.3	21.9	18.0	19.3	**16.8**	19.5	22.7	19.3
Köppen-Geiger climate E																
ALE	51.6	48.6	48.5	44.8	50.3	43.5	49.8	48.4	34.1	31.5	27.0	29.2	**25.7**	26.5	35.8	26.2
DOM	29.1	20.4	33.6	29.1	29.5	21.2	35.5	27.1	14.5	13.7	12.4	12.9	11.8	13.6	15.7	**11.1**
EUR	25.4	29.2	30.5	29.0	31.1	25.6	31.2	30.1	24.6	19.4	19.6	19.0	19.0	21.4	22.1	**15.9**
GVN	62.1	45.3	54.7	46.4	52.7	43.3	58.7	50.8	30.7	29.8	24.7	24.3	23.2	25.2	35.3	**22.9**
NYA	68.5	64.3	60.0	63.0	51.9	51.6	49.3	55.6	46.5	46.3	41.3	44.1	39.6	39.4	41.6	**38.5**
SON	48.6	40.0	48.0	47.6	39.1	36.6	43.6	43.1	37.5	30.8	26.9	28.1	**25.9**	29.5	30.8	26.8
SYO	51.0	43.8	48.4	44.5	46.6	42.8	52.1	47.5	30.0	30.2	25.1	25.9	**23.8**	24.5	34.8	24.2
TIK	32.5	30.4	36.3	32.9	29.9	29.8	31.0	36.1	27.4	24.3	24.3	24.3	23.3	29.9	24.9	**23.1**

6. Conclusion

The separation of solar radiation components has attracted considerable interest during the last six decades. Until recently, nearly all models presented in the literature have used relatively simple transfer functions indirectly relating GHI to the diffuse fraction, K, through the clearness index, K_T. In many scientific disciplines and in the everyday practice of solar engineering, this type of calculation is of critical importance and needs to be done routinely at a large number of sites. This highlights the need to investigate new avenues that have the potential to improve the accuracy of the separation procedure beyond the current methods, while maintaining a minimal model implementation effort. One of these avenues consists in using machine-learning (ML) techniques, which are now becoming prevalent in data-driven problems.

In general, ML techniques are most powerful when there is a lot of information available and the hidden relationship between inputs and outputs is complex. In the separation of GHI, although the relationship between GHI and the diffuse fraction is often complex, the amount of significant information (observed variables) at each time step is limited. Thus, ML techniques miss some of their most potential strengths, although they can still outperform conventional techniques.

Here, three novel global separation models (N1–N3) based on well-established basic artificial neural network (ANN) architectures have been developed. N1 requires only three inputs: solar zenith angle, the 1-min clearness index within the preceding 30-min time window, and the Köppen–Geiger climate class, which recently became popular to improve performance in conventional separation models. N2 is a simpler, climate-independent version of N1. N3 is based on N2 but also requires the clear-sky index (i.e., the ratio between GHI and its ideal clear-sky counterpart). The three new models have been compared to 13 conventional separation models known for their high performance. To that effect, a large database of ≈64 million 1-min irradiance data points from 117 high-quality radiometric world stations has been assembled. Various statistical metrics have been used to evaluate the individual performance of the models and to rank them impartially with the best-known methods.

In general, the performance of N1–N3 has been found to be comparable to, or better than, that of the best conventional models, led by those in the GISPLIT family. N3 has been found to be more effective than N1, indicating that the clear-sky index has a more positive impact than the climate class segregation used in N1. Over the whole database, excluding polar sites, the 1-min DNI N3 predictions are affected by a low RMSE of ≈14%, compared to ≈16% for N2 and N3, and ≈23%, ≈19%, and ≈16% for Perez2, Yang5, and G3, respectively.

Based on the large validation database used here, it is concluded that N3 is a dominating separation model by a small but significant margin over the best non-ML model (G1). It also covers a wider range of observed K_T–K values than any other model, and generally provides a better fit to DNI observations, particularly under cloudless conditions. Under scattered clouds and cloud enhancement conditions, when solar irradiance is highly variable, N3 provides the highest accuracy, indicating that it successfully draws valuable variability information from the observed K_T values during the preceding 30-min time window. This approach is similar to the one adopted in GISPLIT, with the difference that the latter depends on CAELUS to perform the sky-type classification, whereas N3 somehow manages this internally through the sheer power of its ML underpinning. In contrast, older models that do not consider any measure of temporal variability are comparatively inaccurate under such circumstances.

From a historical perspective, a significant increase in model performance has been observed since Engerer2 was published in 2015. In fact, the DNI RMSE has decreased from ≈24% with Engerer2, to ≈16% with GISPLIT and ≈14% with N3. Overall, these results indicate that the best conventional separation models have reached a level of maturity and sophistication that makes them competitive against many ML models, which are not always able to surpass the conventional ones and, if so, only by a narrow margin.

A handicap of ML for GHI separation is that the number of input explanatory variables to the models must be kept to a minimum to maximize their usability (e.g., at remote locations) and ease of use, which means that ML models cannot exploit all their potential. The accuracy increase normally expected with sophisticated ML approaches will likely be impaired by such a reduced number of variables and will likely result in only marginal improvements that might not be justified by the increase in complexity. To exploit the full potential of such complex ML approaches, the set of input features must be increased, which comes at the expense of reduced model usability. However, this could constitute the best solution for local applications that require maximum accuracy.

Although it is very likely that more complex ML models might overpower N3 in terms of prediction accuracy, such apparent improvements could be counterproductive for this application, where simplicity, usability, and execution speed are of paramount importance in practice.

Table A.3
Same as Table A.1 but for the INDEP dataset.

Site	P2	E2	PB	AB	S3	Y4	M1	M2	Y5	G1	G2	G3	G4	N1	N2	N3
Köppen-Geiger climate A																
CHI	8.3	0.9	−1.9	−6.1	−4.9	−2.5	−3.9	−2.7	−2.7	0.8	1.7	0.9	1.8	**−0.1**	−4.3	1.6
DAR	15.5	5.5	1.2	−1.4	−3.8	**−0.5**	−3.8	−0.5	−0.5	1.1	1.4	1.0	2.0	4.7	−0.7	4.5
FEN	16.8	18.3	5.4	5.8	2.0	14.7	1.7	5.8	5.0	3.7	**0.5**	−0.9	1.2	9.6	−3.1	−0.6
GAN	20.5	2.2	2.5	−3.1	−0.5	**−0.4**	−2.3	1.6	−1.5	4.1	2.0	2.3	1.4	−1.2	−6.8	0.4
HAN	24.2	9.8	10.5	3.1	7.3	8.9	5.0	9.5	7.0	8.1	5.3	6.0	5.4	6.8	**−1.4**	3.6
KDO	24.6	6.3	9.4	**1.2**	5.4	4.0	2.7	7.6	2.6	6.9	4.7	5.3	4.5	3.3	−3.0	3.1
MIY	24.8	14.9	14.9	7.9	8.1	5.2	6.5	12.1	5.9	5.5	5.0	4.3	4.3	8.6	5.9	**3.7**
MLE	27.7	8.8	5.7	1.6	4.2	5.0	2.2	4.7	3.8	8.5	5.5	6.1	5.0	6.1	**−1.1**	3.7
TOW	8.3	−1.2	9.4	−6.6	3.3	−0.7	3.7	3.5	1.1	2.1	2.0	2.0	1.9	**0.3**	−1.5	1.4
Köppen-Geiger climate B																
ADE	8.0	2.2	11.9	−2.7	6.2	**0.3**	6.8	6.6	3.5	3.0	5.2	3.4	5.2	1.6	0.7	2.6
ADR	7.3	16.0	27.2	9.6	23.3	12.2	20.5	22.2	7.0	5.4	7.1	5.5	7.4	17.8	17.0	**3.6**
ALB	3.7	−3.6	15.6	−9.8	6.3	−2.4	10.3	6.2	**−0.1**	−0.9	2.1	−0.8	1.9	−1.6	−2.3	−0.7
ARI	4.8	−1.6	14.3	−6.8	8.0	−1.7	8.1	5.8	0.4	1.9	3.6	2.2	3.6	1.2	**0.3**	1.8
BRO	3.6	−5.4	4.3	−10.4	−0.8	−3.1	−0.7	−1.2	−2.1	−0.6	0.2	−0.8	**−0.1**	−5.0	−4.6	−1.5
GAB	2.5	−4.7	6.1	−9.2	0.4	−1.6	3.0	0.5	**−0.1**	0.5	2.6	0.7	2.7	−2.2	−2.5	1.1
HAF	3.3	−3.0	13.0	−8.8	5.4	**0.3**	7.6	4.7	2.7	1.8	4.1	2.2	3.9	−1.2	−1.8	1.4
JOR	1.1	2.6	17.0	−3.6	12.1	3.9	12.7	9.8	**−0.2**	2.3	4.7	2.6	4.8	6.5	5.8	1.6
LAS	7.0	**0.9**	16.5	−4.4	10.5	1.5	10.7	8.2	3.8	4.2	6.2	4.6	6.0	3.3	2.0	3.9
LOY	4.6	−1.4	12.0	−5.6	5.6	**0.6**	6.0	4.9	2.9	1.8	3.9	2.2	3.8	−0.8	−1.4	2.3
MIS	6.1	2.6	16.1	−3.3	10.8	**2.3**	11.8	9.5	4.3	4.3	6.4	4.5	6.3	4.9	4.1	3.8
OUJ	7.0	**2.5**	9.6	−3.4	7.3	3.7	8.1	5.8	5.7	4.1	6.1	4.2	6.1	4.1	3.4	3.5
PAN	12.8	5.0	11.1	−2.1	4.9	1.4	4.4	6.2	1.4	2.2	3.4	1.6	2.6	1.6	**1.0**	2.7
POR	2.8	−3.7	4.6	−8.4	−2.1	−2.6	−0.1	**−0.0**	0.4	−0.4	2.2	−0.3	1.9	−4.5	−5.2	−0.3
RVD	0.2	−5.8	9.7	−11.0	3.9	−2.7	5.3	1.5	−1.6	−0.3	1.2	**−0.1**	1.2	−1.2	−1.3	−0.7
SAL	6.5	0.2	19.9	−5.6	9.0	**−0.1**	12.3	9.7	3.4	1.4	4.8	1.5	4.1	0.1	−0.8	1.0
SHA	−0.3	9.6	18.2	2.8	15.8	7.8	13.3	13.3	0.6	1.7	2.5	1.5	3.1	13.9	13.7	**−0.1**
SRR	3.8	−1.2	10.5	−7.2	4.9	−3.2	7.6	4.3	**0.1**	−1.1	2.2	−0.5	2.1	−2.0	−3.2	0.7
TAB	6.1	−0.8	7.3	−6.8	4.4	−1.2	4.4	3.0	1.2	2.1	3.6	2.1	3.6	1.0	**−0.0**	1.5
TAT	0.5	3.5	14.6	−2.7	10.1	5.3	10.1	8.9	−1.3	1.0	3.2	0.9	3.3	4.9	4.4	**0.2**
WAG	2.9	−3.7	7.4	−8.8	1.9	−2.7	3.7	1.0	−0.6	−1.0	1.0	−0.4	1.2	−2.1	−2.9	**0.0**
Köppen-Geiger climate C																
CAH	25.3	12.3	9.1	6.1	4.5	3.4	**1.4**	6.6	3.9	5.4	3.5	4.0	2.9	1.8	2.7	4.2
CAP	12.6	10.6	15.7	5.2	8.3	4.2	9.4	10.5	6.1	5.0	4.1	6.0	4.3	**2.7**	3.6	6.5
CAS	7.3	1.3	9.4	−5.6	4.3	**−0.0**	4.3	4.1	0.0	0.5	−0.5	0.4	−0.5	−0.4	−2.0	0.1
CHB	35.5	27.6	28.2	20.7	24.2	17.4	20.4	24.8	18.6	21.1	20.7	19.8	19.9	22.4	21.3	**17.3**
CHL	1.6	−4.2	−4.7	−9.4	−9.0	−5.8	−7.2	−5.9	−6.0	−4.0	−7.0	−3.7	−7.2	−6.1	−7.1	**−0.5**
CHO	3.1	−3.0	−1.8	−8.4	−5.4	−3.6	−3.8	−3.5	−1.4	−1.1	−3.8	**−0.8**	−3.9	−3.7	−4.5	1.1
DUR	5.7	−1.9	5.5	−7.6	−0.6	−1.2	0.4	0.7	−1.6	0.1	−1.8	**−0.0**	−1.9	−3.8	−4.7	−0.3
FUU	22.3	20.0	17.1	13.7	13.3	12.4	11.7	14.0	13.6	10.9	**9.4**	10.9	9.8	13.6	14.0	11.0
JAE	6.6	**0.2**	7.3	−5.6	5.1	0.9	5.7	3.6	3.1	2.9	2.4	3.1	2.3	1.6	0.5	2.7
KAA	6.3	**0.1**	−0.7	−5.2	−5.6	−2.9	−4.9	−1.8	−3.3	−0.5	−3.7	−0.4	−4.7	−4.6	−5.6	1.4
KAO	5.9	−0.5	**0.1**	−6.1	−3.8	−2.0	−2.8	−1.5	0.5	1.0	−1.6	1.0	−2.0	−3.3	−4.2	1.2
KAS	10.8	3.7	10.7	−4.7	4.0	1.1	6.4	7.6	**0.9**	4.3	2.5	4.0	1.7	−2.3	−3.2	2.0
KWA	10.2	0.7	3.2	−4.6	1.6	−0.8	−0.2	0.7	−1.0	2.9	2.2	2.7	2.2	0.8	**0.1**	1.4
LOC	5.7	−1.1	6.8	−6.8	3.1	−4.9	0.9	2.2	−4.3	−0.7	**−0.3**	−1.2	−0.9	−1.0	−2.9	−2.8
LUS	6.1	0.8	4.0	−6.3	−0.6	**−0.4**	1.3	1.2	−0.8	0.7	−1.3	1.1	−1.3	−3.0	−3.4	1.2
MEL	6.0	1.3	6.5	−4.8	1.9	−2.0	2.8	2.0	−1.0	0.4	−0.2	1.1	**0.0**	−1.5	−1.5	1.5
MIL	12.4	3.9	7.3	−3.3	5.0	2.7	4.2	4.2	3.1	4.3	3.2	4.0	2.9	2.3	**0.0**	3.2
MUT	2.1	−3.3	−3.1	−7.9	−8.4	−5.4	−7.0	−3.8	−5.7	−3.1	−6.7	−3.0	−7.3	−6.7	−8.4	**−1.4**
MZU	7.5	2.8	14.2	−4.4	3.2	**−0.2**	6.3	7.7	−0.2	0.8	−1.3	1.2	−1.6	−4.4	−4.2	1.0
ORE	8.7	2.5	8.8	−5.1	4.7	−1.4	3.1	2.7	1.2	2.0	1.6	1.7	1.3	**−0.6**	−1.8	0.8
PRE	3.5	−3.3	6.6	−8.2	1.2	−1.2	3.6	1.2	0.6	−0.4	−2.3	**0.1**	−2.1	−1.0	−1.8	1.4
ROC	7.5	−1.5	6.4	−7.8	1.2	−3.3	1.3	1.5	−3.7	−0.2	−1.1	**0.0**	−0.8	−2.1	−2.1	0.7
SEA	3.2	−2.8	10.5	−10.3	1.4	−3.2	3.4	3.3	−1.3	**−1.0**	−2.8	−1.2	−3.3	−7.3	−9.0	−2.7
STE	1.3	−5.8	6.4	−10.8	**0.2**	−3.9	2.1	−0.3	−2.1	−1.5	−2.2	−1.0	−2.0	−3.6	−4.2	−0.9
STR	10.4	3.0	12.0	−3.5	5.9	0.3	6.7	6.7	1.1	1.0	0.6	0.8	0.3	**0.0**	−1.0	0.5
VUW	3.1	−3.3	2.2	−8.9	−4.2	−3.9	−2.0	−1.7	−0.7	**−0.5**	−3.4	−0.5	−3.4	−4.8	−6.0	−1.0
Köppen-Geiger climate D																
BIS	6.4	1.1	17.8	−5.0	9.2	1.2	11.3	8.9	2.2	0.1	**−0.0**	0.2	−0.0	−3.6	−1.4	0.1
DAO	8.2	6.3	15.7	−2.1	8.0	**0.8**	13.2	10.3	2.8	4.0	5.5	3.2	3.5	−2.0	1.2	2.9
KAZ	7.4	6.0	19.3	−2.2	11.0	0.9	13.3	13.1	2.5	1.6	2.8	1.9	2.0	−2.4	**−0.8**	1.6
KIR	14.1	11.8	12.8	2.8	11.3	1.6	10.2	9.7	6.4	5.5	7.3	6.2	6.4	**0.5**	1.1	6.4
LYN	7.1	3.9	6.4	−5.5	3.1	1.6	4.1	2.6	3.1	**0.4**	−0.7	0.7	−0.6	−3.4	−1.9	1.6
MAD	8.5	0.6	12.9	−5.8	5.4	−0.9	7.0	6.1	0.1	−0.2	−0.3	**−0.0**	−0.5	−4.9	−2.9	0.2
NOR	10.5	5.6	3.5	−2.4	3.7	−1.5	1.9	1.3	1.3	2.5	3.1	3.2	3.2	−1.8	**−0.8**	3.5
ODE	2.8	−2.2	4.6	−8.3	2.8	−1.8	5.3	1.4	−1.7	−1.2	−1.0	−0.6	−1.5	−5.7	−3.4	**−0.1**
VIS	8.4	3.0	4.3	−2.9	4.4	−1.7	1.9	1.3	**0.1**	1.4	1.6	2.0	1.9	−1.8	−0.5	1.6

Table A.4
Same as Table A.1 but for RMSE and the INDEP dataset.

Site	P2	E2	PB	AB	S3	Y4	M1	M2	Y5	G1	G2	G3	G4	N1	N2	N3
Köppen-Geiger climate A																
CHI	25.9	24.6	22.7	28.4	20.5	20.1	19.4	21.9	19.0	19.3	18.9	18.4	17.9	15.6	18.4	**15.0**
DAR	32.2	27.4	25.3	28.2	22.3	21.6	21.3	24.5	20.1	19.9	18.8	18.8	18.0	16.7	17.8	**15.8**
FEN	43.6	38.0	26.1	34.8	25.2	33.6	23.1	26.9	24.5	24.8	22.7	23.1	21.5	25.1	26.3	**19.6**
GAN	34.6	22.5	21.7	23.6	19.8	18.4	18.3	21.4	18.3	18.1	17.2	16.7	16.3	15.2	18.5	**14.7**
HAN	38.1	24.7	22.7	23.9	21.0	21.7	18.0	22.7	20.0	19.9	17.6	17.5	16.9	18.3	17.6	**15.5**
KDO	38.6	23.8	23.0	23.6	20.7	20.6	18.4	22.4	19.6	19.8	18.3	18.0	17.4	16.8	17.6	**16.3**
MIY	43.8	38.9	34.8	37.5	28.7	31.2	26.8	33.2	30.3	26.5	26.8	25.1	25.7	25.2	24.5	**22.3**
MLE	43.4	25.5	24.3	25.0	23.0	21.3	19.9	25.1	20.2	21.3	18.8	18.5	17.5	18.4	18.4	**16.2**
TOW	19.1	18.4	20.2	21.1	15.2	13.7	14.8	17.1	14.0	12.8	12.7	12.1	12.1	11.0	11.0	**9.9**
Köppen-Geiger climate B																
ADE	19.3	22.0	25.4	23.9	19.4	16.8	19.1	21.8	17.7	15.0	16.0	14.7	15.5	14.1	13.1	**13.0**
ADR	20.8	28.1	34.7	26.2	31.0	26.9	28.4	31.3	22.0	17.5	18.3	16.8	17.8	24.7	24.7	**15.9**
ALB	12.4	15.6	22.4	20.3	14.4	12.9	16.5	16.3	12.7	11.0	10.4	10.6	10.1	9.5	9.9	**8.7**
ARI	12.2	13.1	19.1	15.6	14.2	10.1	13.3	13.4	10.4	9.0	9.6	8.7	9.2	8.3	7.8	**7.2**
BRO	15.7	15.3	14.0	19.1	12.5	11.0	10.9	12.7	10.9	9.4	9.1	9.1	8.9	12.0	11.0	**7.9**
GAB	13.4	15.9	15.5	19.4	12.2	11.4	11.6	13.1	11.0	10.7	10.6	10.4	10.4	9.8	9.8	**8.3**
HAF	12.3	14.4	19.4	18.1	12.6	11.4	13.4	14.5	11.9	10.1	10.5	9.8	10.3	8.6	8.9	**8.5**
JOR	11.5	15.7	23.3	17.5	18.4	14.2	18.0	18.1	13.1	10.2	10.8	9.9	10.6	13.0	13.1	**9.0**
LAS	17.0	17.3	24.6	18.7	19.8	15.5	19.6	19.1	16.0	15.2	15.9	15.0	15.5	14.5	14.2	**13.6**
LOY	16.3	17.9	22.1	19.0	17.4	13.9	16.4	17.6	14.9	12.3	12.8	12.2	12.6	12.8	12.0	**10.7**
MIS	15.8	18.1	24.1	19.9	18.7	16.3	18.8	19.7	16.2	13.7	14.2	13.2	13.8	14.2	14.6	**11.4**
OUJ	16.6	18.8	19.2	20.5	16.6	16.1	15.9	17.7	16.2	13.2	13.6	12.6	13.4	13.4	13.8	**10.9**
PAN	27.8	24.9	24.7	25.7	20.0	18.1	18.7	22.0	18.3	17.1	17.2	16.4	16.8	16.7	16.1	**14.1**
POR	22.0	25.0	23.7	28.0	20.1	19.2	19.3	22.1	19.5	17.2	17.0	16.8	16.8	18.2	17.5	**14.6**
RVD	8.7	12.2	14.6	16.7	10.1	8.8	10.3	10.3	9.0	6.9	7.1	6.7	6.9	6.9	6.8	**5.9**
SAL	18.4	20.5	29.1	23.7	19.3	17.3	21.2	21.6	17.7	14.4	15.1	14.0	14.5	13.0	12.8	**12.0**
SHA	12.2	14.4	21.9	12.6	19.6	15.6	16.7	17.5	10.7	10.0	10.2	9.7	10.1	16.9	16.9	**9.0**
SRR	17.2	19.3	23.2	22.9	17.8	16.5	19.0	18.8	16.0	14.5	14.8	13.7	14.0	13.2	13.1	**11.3**
TAB	15.7	17.2	18.7	20.4	14.9	14.7	14.8	16.5	14.4	12.3	12.4	11.5	11.9	11.5	11.8	**9.9**
TAT	13.6	17.3	22.3	18.1	17.8	15.5	16.9	18.6	14.2	11.0	11.2	10.5	10.9	12.4	12.0	**9.0**
WAG	13.9	17.6	19.1	21.2	14.3	13.0	14.1	15.8	12.8	11.5	11.5	11.1	11.1	10.8	10.5	**9.4**
Köppen-Geiger climate C																
CAH	45.4	36.3	32.5	34.7	28.3	28.8	26.4	31.5	28.1	26.0	25.2	24.1	24.2	23.6	23.6	**21.5**
CAP	31.9	37.4	38.4	37.0	30.1	28.2	30.4	34.9	29.0	25.6	25.1	25.3	24.6	**22.3**	23.1	23.4
CAS	19.5	20.7	23.7	23.1	17.8	16.3	17.2	20.7	16.2	14.2	14.0	13.4	13.4	13.6	14.1	**11.5**
CHB	55.3	46.5	46.0	41.6	40.9	35.1	35.6	42.8	34.6	35.9	36.1	34.3	35.1	37.6	36.1	**30.7**
CHL	21.9	23.1	20.2	26.4	20.2	18.9	18.3	19.7	17.9	18.7	20.0	18.1	20.0	16.2	17.7	**14.0**
CHO	20.5	21.1	17.4	24.2	16.9	16.7	15.3	17.1	15.5	16.5	17.3	16.0	17.2	13.9	14.9	**12.7**
DUR	23.9	24.9	21.9	28.3	17.3	18.2	16.4	20.3	18.1	16.6	16.7	15.9	16.3	15.7	17.2	**13.8**
FUU	46.0	46.5	41.1	42.3	35.2	35.7	33.7	38.8	34.8	30.7	29.6	29.6	28.9	30.9	31.1	**27.5**
JAE	16.1	18.0	17.1	20.0	14.9	14.4	14.4	15.9	14.6	12.7	12.1	12.1	11.7	11.9	11.7	**10.3**
KAA	26.7	25.1	20.6	27.5	19.8	20.0	18.3	20.1	19.3	20.5	21.3	20.1	21.5	17.2	18.6	**16.0**
KAO	23.5	22.4	18.5	25.3	17.3	17.6	16.0	18.1	16.8	17.3	17.7	16.8	17.5	14.7	15.6	**13.5**
KAS	25.3	23.4	25.5	27.2	18.8	19.4	19.6	23.3	18.3	18.3	18.1	17.4	16.9	15.5	16.2	**14.5**
KWA	24.1	22.9	19.8	25.5	16.3	18.6	16.1	18.8	18.5	15.7	15.2	15.0	14.7	13.4	14.0	**13.0**
LOC	20.1	20.7	20.6	24.2	17.3	20.4	16.6	18.9	19.7	15.3	15.0	14.5	14.4	14.8	14.9	**13.4**
LUS	22.1	22.4	19.6	26.6	16.0	17.4	15.5	18.4	16.3	16.8	17.0	16.4	16.6	15.1	15.7	**13.5**
MEL	21.0	25.0	26.0	28.4	20.3	18.7	20.0	22.8	18.8	17.0	17.0	16.3	16.3	14.4	14.7	**13.9**
MIL	26.3	26.1	25.9	28.2	21.6	22.4	20.6	24.5	21.6	18.6	17.9	17.8	17.4	16.8	17.1	**15.7**
MUT	24.9	24.0	20.1	26.1	21.4	20.4	19.4	19.8	19.5	21.1	22.6	20.7	22.8	17.7	20.0	**16.1**
MZU	24.9	25.4	28.2	28.0	19.2	20.3	20.4	24.0	19.3	19.4	19.5	18.8	18.9	17.0	17.6	**15.9**
ORE	25.2	27.0	26.5	30.0	20.9	21.1	20.6	23.6	22.5	19.0	18.6	18.6	17.9	16.3	17.0	**16.1**
PRE	13.8	16.4	16.1	19.6	12.2	11.8	12.0	13.1	11.2	11.3	11.4	10.8	11.2	9.7	10.1	**8.9**
ROC	18.8	18.3	19.4	21.7	14.9	14.1	14.4	16.6	14.3	12.7	12.9	12.1	12.3	11.0	11.0	**9.6**
SEA	21.7	25.3	29.6	29.5	20.4	20.2	21.4	25.5	20.6	17.4	17.8	17.1	17.5	17.1	19.2	**14.4**
STE	12.3	17.2	16.2	21.1	12.5	12.3	12.2	14.1	12.1	10.7	10.8	10.3	10.5	10.3	10.7	**9.1**
STR	25.4	23.6	26.6	26.7	20.1	19.2	20.0	23.0	19.0	16.8	16.5	15.9	15.8	15.1	15.3	**13.9**
VUW	25.8	27.2	25.5	30.4	24.3	23.1	23.1	23.6	21.9	22.0	23.1	21.8	22.9	21.0	23.4	**20.2**
Köppen-Geiger climate D																
BIS	18.9	21.1	28.7	23.8	19.7	17.4	21.2	22.4	17.8	14.5	14.2	14.1	13.8	14.4	14.1	**12.1**
DAO	28.4	28.8	32.4	33.8	26.0	25.0	30.6	28.5	25.4	21.3	22.2	20.2	20.9	20.3	18.9	**17.1**
KAZ	23.0	25.8	32.1	28.6	24.0	22.8	25.3	27.9	22.8	19.4	19.5	18.7	19.0	17.8	17.3	**15.9**
KIR	39.0	39.8	41.9	42.6	35.7	31.9	35.4	38.8	32.7	29.2	30.1	28.3	28.8	25.4	25.8	**24.2**
LYN	24.0	26.4	27.0	29.5	20.0	20.1	19.3	25.1	19.9	18.4	18.2	17.7	17.8	18.0	17.6	**15.2**
MAD	22.9	23.6	28.2	27.2	20.2	19.0	21.1	23.3	19.3	16.4	16.0	15.7	15.5	16.4	15.6	**13.4**
NOR	29.3	30.5	29.7	33.1	25.7	25.3	24.2	27.8	25.1	22.7	22.6	21.9	21.8	19.8	19.8	**18.9**
ODE	15.7	19.9	19.5	23.2	16.0	16.7	17.3	18.7	16.7	14.2	14.2	13.7	13.8	14.5	13.4	**11.7**
VIS	23.8	25.3	25.6	27.0	21.7	22.0	20.7	23.7	21.9	18.8	18.8	18.2	18.2	16.7	16.7	**16.1**

Table A.5
DIF MBE in percent by site in each climate class, relative to the mean observed DIF, for the VALID dataset and for all separation models. The lowest error for each site is bold-faced.

Site	P2	E2	PB	AB	S3	Y4	M1	M2	Y5	G1	G2	G3	G4	N1	N2	N3
Köppen-Geiger climate A																
BER	−19.2	−13.3	−36.0	−6.2	−18.1	−8.9	−22.5	−25.6	−8.3	−5.6	−8.6	−5.8	−7.2	−6.7	**−3.9**	−4.5
COC	−21.2	−6.5	−5.6	−1.7	1.6	−1.0	3.7	−5.0	1.1	0.4	−0.4	**−0.2**	−1.4	−2.4	3.0	−1.4
DAR	−13.5	2.5	**−0.4**	10.5	8.1	3.7	9.0	1.3	1.5	5.9	4.5	6.2	4.4	−2.7	8.0	4.6
DWN	−13.6	**1.4**	2.5	8.9	8.1	3.5	10.9	3.5	1.4	6.0	4.9	6.2	4.7	−3.2	6.7	5.2
ISH	−15.7	−11.8	−9.0	−7.3	−3.6	−7.9	−1.4	−8.0	−6.2	−0.8	−1.8	**−0.7**	−1.9	−7.2	−1.9	−1.2
KWA	−26.6	−11.5	−29.6	−5.4	−11.7	−5.7	−14.0	−22.2	−3.7	−3.6	−4.8	−2.5	−3.4	−6.4	−1.6	**−1.2**
MAN	−26.9	−6.0	−2.6	−2.0	4.4	**0.1**	6.6	−2.1	1.6	−5.0	−4.5	−3.8	−4.1	−1.4	4.8	−2.7
MNM	−19.0	−0.3	−0.3	4.5	5.6	2.9	9.6	0.8	**0.1**	3.6	3.6	2.4	1.6	1.6	8.2	1.2
NAU	−25.4	−2.4	−4.3	4.3	6.1	4.3	6.3	−3.2	6.2	0.5	0.9	1.2	0.7	2.8	8.6	**−0.1**
TIR	−9.8	−16.2	−3.8	−11.4	0.4	−11.1	2.1	−3.8	−10.7	1.3	0.3	2.3	−0.4	−8.7	−0.9	**0.0**
Köppen-Geiger climate B																
ASP	**3.5**	35.6	8.0	55.6	13.6	27.5	4.6	18.6	24.6	10.3	4.6	9.2	4.3	17.6	14.7	9.9
BOS	−7.3	0.8	−36.0	14.1	−15.7	1.6	−25.9	−17.7	−3.5	1.1	−5.3	0.8	−4.3	0.4	1.4	**−0.1**
DAA	2.0	31.5	−4.1	60.1	4.5	24.2	−12.0	8.6	19.2	10.7	3.3	9.4	**1.5**	18.4	18.5	8.2
DRA	−2.5	16.3	−50.6	35.4	−19.8	6.0	−32.6	−16.1	**1.2**	2.6	−5.3	1.8	−4.2	4.9	4.5	3.8
FPE	−11.1	−7.1	−31.8	3.4	−18.9	−8.0	−22.7	−20.0	−7.5	−2.5	−8.6	−1.9	−7.5	−4.2	−3.5	**−0.6**
GOB	12.9	23.8	−8.1	41.5	−2.2	13.1	−7.2	3.2	35.8	4.4	−1.6	4.0	−1.5	3.2	**−1.3**	10.4
PTR	−16.5	−2.3	−2.3	4.6	8.2	4.8	6.9	−1.3	6.3	2.1	**−0.4**	0.6	−0.7	8.0	6.4	−0.9
SBO	29.6	5.5	−19.4	17.6	−7.2	−4.4	−16.6	−9.2	12.4	17.9	7.5	14.9	5.9	**0.1**	−1.7	13.8
SOV	26.1	−17.9	−40.5	−7.0	−33.2	−25.3	−37.0	−30.4	−9.3	4.9	**−1.9**	2.4	−2.0	−25.8	−27.9	5.2
TAM	11.5	8.8	−14.1	23.9	−6.6	4.1	−18.7	−3.9	3.8	14.3	**3.1**	13.3	3.1	5.1	8.1	14.0
Köppen-Geiger climate C																
BIL	−11.9	**0.2**	−18.6	7.7	−5.9	−3.5	−8.6	−9.2	−6.7	1.7	3.8	1.2	3.6	2.0	3.4	0.5
CAB	−11.6	−10.6	−5.2	−5.0	−5.5	−6.4	−3.8	−4.9	−7.5	−3.3	**−2.3**	−3.6	−2.3	−5.4	−4.4	−4.3
CAR	−5.1	3.3	1.9	10.9	4.5	**0.7**	4.7	3.5	−2.8	1.9	4.0	1.7	4.2	3.3	5.5	2.3
CLH	−19.7	−7.4	−23.0	**−0.7**	−13.9	−8.7	−12.0	−16.5	−5.2	−6.1	−5.7	−6.0	−5.4	−3.2	−1.2	−2.4
CNR	−7.7	−5.2	−2.6	1.6	−0.8	−2.0	−1.2	−1.8	−1.8	**−0.2**	1.0	−0.6	1.0	−1.4	−1.2	−0.8
E13	−12.2	−1.0	−14.0	7.9	−5.3	−3.6	−7.7	−7.9	−7.2	0.6	2.4	**0.1**	2.1	0.1	1.4	0.5
FLO	−15.4	−3.9	−9.3	1.2	−1.4	**−0.4**	−1.1	−5.3	0.8	−2.6	−1.8	−2.6	−1.6	1.7	1.9	−1.2
FUA	−8.4	−9.6	−3.8	−5.0	−1.8	−8.1	**0.0**	−3.2	−6.5	−0.5	2.4	−0.8	2.4	−4.4	−3.5	−0.9
GCR	−15.3	−4.9	−50.5	1.9	−20.2	−6.8	−26.8	−27.0	−3.3	1.8	3.9	2.1	4.6	2.2	2.5	**1.5**
IZA	11.2	23.2	−45.4	78.8	−6.6	27.2	−46.5	−14.7	19.5	−9.8	−10.6	−9.6	−9.7	−12.3	**−3.6**	−7.2
LAU	−8.1	−2.7	−3.3	7.8	−1.3	4.4	−4.6	−4.0	3.0	−2.0	−2.4	−2.0	−1.2	2.3	3.3	**−0.5**
LRC	−9.9	−0.9	−4.0	5.0	**0.3**	1.5	2.6	−1.3	3.4	4.3	5.1	4.1	5.0	2.5	3.4	4.1
PAL	−11.3	−8.9	−4.4	−2.4	−3.8	−3.3	−2.4	−4.2	−4.0	−2.0	−1.1	−2.2	**−0.9**	−4.1	−3.6	−3.0
PAY	−14.5	−7.2	−7.8	**−1.1**	−7.3	−5.3	−6.1	−6.4	−4.7	−5.5	−5.1	−6.0	−5.1	−6.0	−4.4	−4.9
SMS	−5.4	3.4	−4.7	11.3	3.9	6.3	1.4	**0.5**	7.4	4.9	6.4	4.0	5.9	6.4	6.2	3.5
TAT	−6.9	−8.7	−2.6	−4.7	−1.5	−4.7	**1.4**	−2.6	−4.2	1.6	3.5	1.5	3.4	−3.3	−2.7	1.8
Köppen-Geiger climate D																
BON	−12.4	−7.1	−28.7	−1.0	−14.6	−6.7	−18.2	−17.9	−5.7	−1.3	1.1	−1.3	1.2	3.5	−1.6	**−0.9**
LIN	−7.9	−8.1	−10.5	−3.1	−4.2	−1.7	−4.4	−6.4	−3.2	1.0	2.0	**0.7**	1.7	0.8	−1.1	−0.8
PSU	−12.3	−10.8	−32.1	−4.5	−16.1	−7.3	−20.8	−21.1	−7.3	−0.7	1.1	−0.5	1.7	**0.3**	−3.1	−0.9
REG	−9.4	−8.5	−17.4	1.7	−11.8	−3.4	−15.9	−13.5	−4.9	−3.4	−4.0	−2.7	−2.8	**0.3**	−3.9	−2.0
SAP	−6.7	−10.8	−3.1	−6.3	−2.7	−6.7	−2.1	−3.6	−7.3	**−0.1**	2.5	−0.6	2.2	−1.6	−5.1	−1.3
SXF	−11.4	−9.9	−47.3	−2.8	−24.8	−12.5	−31.9	−29.0	−11.5	−3.0	**0.5**	−2.4	1.5	3.1	−3.6	−2.0
TOR	−5.9	−4.0	1.9	2.7	0.6	0.9	1.7	2.1	**−0.5**	1.9	2.8	1.7	2.7	3.3	1.2	0.6
XIA	−14.5	−23.1	−25.1	−14.3	−21.8	−22.8	−21.4	−22.1	−13.8	−9.8	**−4.2**	−7.6	−4.2	−7.3	−12.1	−7.9
Köppen-Geiger climate E																
ALE	−16.5	−20.7	−21.9	−16.5	−23.1	−15.6	−25.5	−22.0	−6.2	−11.2	−4.7	−8.5	−4.0	**−3.7**	−13.4	−7.0
DOM	−37.3	−26.8	−74.9	43.3	−61.4	−30.8	−89.0	−53.1	−2.9	−12.0	3.1	−8.6	**0.4**	−3.8	−9.6	1.3
EUR	−4.6	−11.7	−9.4	−3.2	−17.8	−8.9	−16.2	−10.9	4.7	−1.8	6.2	−0.4	5.6	5.2	−5.5	**0.2**
GVN	−25.0	−26.4	−36.8	−13.6	−36.9	−23.8	−45.1	−33.2	−8.1	−13.7	−1.1	−4.5	**0.3**	−6.2	−18.8	−4.2
NYA	−8.1	−7.9	**−1.1**	−6.3	−4.1	−3.2	−2.2	−1.5	1.5	−4.5	−1.2	−3.6	−1.6	1.8	−2.7	−3.1
SON	−13.7	−12.9	−25.9	−1.0	−14.7	−6.1	−26.1	−20.6	−8.6	−8.0	1.0	−5.2	**0.3**	2.7	−6.2	−7.2
SYO	−30.9	−27.0	−34.6	−15.7	−41.5	−28.9	−51.4	−33.3	−4.2	−15.8	−1.9	−7.7	**−0.4**	−6.3	−21.1	−9.0
TIK	5.4	**−0.5**	9.4	10.2	7.2	7.9	−1.0	7.5	11.8	4.3	8.1	6.9	8.9	17.1	4.9	10.1

CRediT authorship contribution statement

Jose A. Ruiz-Arias: Writing – original draft, Software, Methodology, Data curation, Conceptualization. **Enrique Domínguez:** Writing – review & editing, Software, Methodology, Conceptualization. **Christian A. Gueymard:** Writing – review & editing, Conceptualization.

Declaration of competing interest

The authors declare that they have no known competing financial interests or personal relationships that could have appeared to influence the work reported in this paper.

Table A.6
Same as Table A.5 but for RMSE.

Site	P2	E2	PB	AB	S3	Y4	M1	M2	Y5	G1	G2	G3	G4	N1	N2	N3
Köppen-Geiger climate A																
BER	41.1	41.0	55.0	40.2	37.1	34.3	40.7	45.7	33.3	28.2	29.2	26.7	27.8	25.4	25.1	**23.5**
COC	47.0	39.5	33.8	38.5	29.5	32.4	30.0	32.9	32.1	29.1	29.0	27.6	27.6	25.2	26.5	**24.3**
DAR	47.8	40.0	31.9	40.7	30.4	32.8	29.0	31.3	31.1	30.2	28.7	28.5	26.9	24.8	27.8	**24.2**
DWN	46.9	39.4	33.1	39.7	31.5	33.2	31.7	32.4	31.8	30.5	29.3	28.8	27.4	24.7	27.5	**23.6**
ISH	40.7	40.4	33.3	37.8	28.9	31.9	28.3	32.9	30.7	26.5	26.9	25.5	25.8	26.1	26.4	**22.7**
KWA	49.3	39.6	49.8	38.8	34.2	35.3	35.8	43.0	33.9	29.7	29.7	27.7	28.2	25.4	25.4	**24.9**
MAN	53.3	37.4	34.8	36.2	30.4	31.7	31.3	32.8	31.0	29.3	28.7	27.0	26.8	**23.4**	25.7	23.8
MNM	45.6	41.3	37.6	40.6	32.2	32.7	35.1	35.7	33.3	30.6	31.4	28.9	29.3	27.3	31.0	**25.8**
NAU	54.7	38.5	38.2	38.5	33.7	34.4	33.6	35.0	33.5	31.4	30.6	29.3	29.0	**25.5**	28.8	26.3
TIR	29.2	35.4	23.0	32.5	23.0	30.8	20.2	24.6	26.8	19.8	18.7	18.7	17.9	22.9	22.1	**17.2**
Köppen-Geiger climate B																
ASP	43.3	63.7	48.2	84.2	41.2	49.0	39.8	45.9	48.5	35.1	33.5	32.7	32.0	36.3	31.7	**28.4**
BOS	35.1	41.6	58.1	49.8	37.9	35.7	45.8	43.5	34.7	30.6	30.6	29.0	28.9	26.9	26.7	**24.4**
DAA	45.2	68.1	53.7	100.7	43.9	55.5	46.9	53.3	53.7	39.1	38.1	37.6	36.2	40.5	38.9	**31.9**
DRA	39.0	50.4	71.7	65.2	42.0	39.4	52.4	49.2	39.7	32.1	31.4	30.0	29.7	29.4	29.2	**26.3**
FPE	39.8	45.7	58.5	47.5	45.0	40.4	48.9	49.7	41.2	30.7	33.7	29.4	32.0	31.2	29.5	**25.8**
GOB	39.8	54.2	45.4	70.1	36.3	41.6	37.4	42.7	62.0	28.8	28.8	27.9	27.6	27.9	26.9	**26.8**
PTR	43.0	38.9	33.2	39.8	31.2	29.8	29.9	31.8	29.8	28.3	28.1	26.9	26.2	28.6	25.5	**22.7**
SBO	44.7	48.7	46.1	52.9	37.6	40.7	40.6	42.1	43.4	34.1	27.9	31.4	**26.5**	32.0	33.0	28.6
SOV	37.9	40.3	57.2	38.8	47.9	43.9	51.0	47.4	31.4	22.0	20.4	20.1	**19.3**	39.4	43.1	20.2
TAM	38.2	50.9	44.0	66.1	34.7	40.4	41.8	40.7	39.8	34.8	29.2	34.4	**28.7**	33.0	33.1	30.3
Köppen-Geiger climate C																
BIL	42.2	42.5	50.4	42.2	34.5	33.8	36.5	40.6	34.0	28.1	28.4	26.9	27.3	27.0	27.2	**23.4**
CAB	33.7	39.2	31.4	37.6	27.7	31.5	27.0	31.1	31.0	25.1	24.6	24.1	23.6	23.7	23.6	**21.1**
CAR	34.7	42.0	34.7	43.5	31.1	31.9	30.3	34.8	32.2	26.9	27.3	25.7	26.2	26.1	27.0	**22.5**
CLH	45.2	44.9	49.9	44.4	38.7	42.0	39.5	45.8	41.0	31.2	30.4	29.7	29.2	28.1	28.2	**26.2**
CNR	32.1	39.8	33.0	40.8	28.8	31.3	29.2	32.7	31.0	27.1	26.9	25.9	25.8	23.7	23.6	**21.2**
E13	42.1	43.9	42.1	45.1	33.3	36.0	34.0	38.5	36.5	28.4	28.6	27.3	27.5	27.5	27.3	**24.4**
FLO	40.1	38.6	41.8	39.4	29.4	31.5	31.7	35.7	32.0	27.1	26.8	25.7	25.3	23.0	23.3	**21.3**
FUA	33.1	35.1	29.2	33.1	26.2	31.6	26.2	29.4	28.7	22.8	22.4	21.8	21.4	24.6	24.0	**19.5**
GCR	47.0	42.1	71.1	41.0	40.3	33.9	45.6	49.9	32.5	28.7	29.0	27.8	28.3	27.2	27.2	**23.2**
IZA	65.0	81.3	82.8	143.7	75.6	86.2	82.6	73.0	81.8	57.1	51.7	51.9	**46.6**	60.6	61.4	52.1
LAU	35.9	41.1	44.8	51.9	33.0	36.0	35.5	39.6	36.3	30.7	30.2	28.9	28.3	25.4	25.2	**23.5**
LRC	38.4	38.0	31.4	38.8	27.1	30.6	27.8	29.6	30.9	26.8	26.9	25.6	25.8	24.3	24.3	**23.3**
PAL	33.7	37.2	30.0	37.1	26.3	29.0	25.9	28.8	28.2	25.2	25.1	24.1	24.0	23.3	22.7	**20.4**
PAY	36.9	40.5	35.4	40.4	29.9	32.9	30.6	34.2	33.2	27.7	27.5	26.5	26.2	25.4	24.6	**22.8**
SMS	36.2	40.8	34.0	47.1	27.6	31.6	27.5	32.4	32.9	27.5	28.1	26.0	26.7	24.7	24.5	**23.1**
TAT	33.8	36.4	28.4	34.7	24.2	29.3	24.0	27.2	27.4	22.9	23.0	22.0	22.3	22.7	22.7	**19.7**
Köppen-Geiger climate D																
BON	37.0	38.3	50.2	38.8	33.6	31.6	36.8	40.3	30.7	24.8	24.4	23.9	23.6	25.2	24.5	**21.8**
LIN	29.2	35.3	33.5	34.8	24.9	27.0	25.4	29.5	26.5	23.7	24.0	22.8	23.0	21.6	20.9	**19.8**
PSU	36.9	40.1	53.6	39.3	35.4	31.5	39.8	43.2	30.8	26.4	26.4	25.3	25.4	23.9	23.4	**21.3**
REG	39.2	45.0	46.7	48.5	40.2	40.3	45.2	43.6	41.2	30.7	31.1	28.7	28.3	30.3	29.8	**25.4**
SAP	30.9	36.6	29.7	34.8	26.0	30.5	26.5	29.4	29.2	24.1	24.2	22.7	22.7	21.5	21.7	**19.3**
SXF	38.6	43.8	67.9	43.7	45.9	38.6	52.3	52.9	38.2	30.2	30.4	29.3	29.3	29.7	28.6	**24.8**
TOR	32.6	37.5	31.9	38.7	27.5	28.8	27.5	30.2	29.0	25.9	25.8	24.5	24.5	24.7	23.6	**21.2**
XIA	30.3	45.4	45.2	39.0	39.4	45.0	38.3	42.0	33.0	24.2	19.9	21.6	**18.8**	23.3	27.9	22.2
Köppen-Geiger climate E																
ALE	41.2	40.8	40.1	39.0	42.8	37.3	44.8	40.9	27.9	26.7	22.5	24.4	**21.3**	22.5	30.5	22.2
DOM	81.3	66.2	102.1	112.7	96.4	71.4	115.2	83.4	49.6	45.8	40.8	42.3	38.0	43.2	49.2	**36.8**
EUR	36.2	41.2	41.9	40.5	42.9	37.1	45.6	41.8	35.8	28.0	29.5	27.3	28.2	31.6	30.4	**22.5**
GVN	59.1	56.2	64.5	60.4	64.2	56.2	75.5	62.4	38.9	37.7	29.3	29.0	**27.6**	31.7	44.3	29.2
NYA	26.7	27.1	24.8	27.1	21.4	21.3	20.5	22.4	18.7	18.8	16.7	17.8	16.1	17.3	17.3	**15.7**
SON	45.5	46.9	56.2	59.5	46.5	42.6	54.6	51.0	42.8	37.5	30.3	32.6	**29.0**	32.5	34.5	31.3
SYO	71.2	65.6	69.7	68.8	73.5	66.1	85.9	70.6	44.7	45.7	34.9	35.9	**32.0**	36.0	53.1	36.9
TIK	40.0	40.4	52.8	49.4	43.3	44.6	47.1	43.7	41.3	32.0	33.7	32.1	32.4	49.9	32.9	**31.3**

Acknowledgments

This work was supported by the project PID2023-149827OB-C21 funded by the Spanish Ministry of Science, Innovation and Universities, the State Research Agency and FEDER (MCIU/AEI/10.13039/501100011033/FEDER,EU). The authors would like to thank the scientists and personnel in charge of the BSRN stations for kindly sharing their datasets, as well as the entities and scientists that shared the INDEP dataset and the members of the Task 16 of the International Energy Agency's Photovoltaic Power Systems Programme that developed the robust quality control algorithm used to produce it.

Appendix. Site-wise performance metrics

See Tables A.1–A.8.

Table A.7
Same as Table A.5 but for the INDEP dataset.

Site	P2	E2	PB	AB	S3	Y4	M1	M2	Y5	G1	G2	G3	G4	N1	N2	N3
Köppen-Geiger climate A																
CHI	−13.2	−3.8	**−0.3**	4.5	6.1	1.6	4.5	0.3	3.3	−1.0	−3.3	−1.6	−3.4	−2.2	3.9	−3.0
DAR	−19.7	−8.0	−4.5	−2.3	4.1	−0.3	4.2	−2.7	1.1	**−0.2**	−1.5	−0.7	−2.5	−6.7	−0.6	−5.8
FEN	−14.1	−16.8	−6.0	−8.9	−2.2	−14.4	−0.5	−7.2	−4.3	−1.9	**−0.2**	0.9	−1.1	−8.9	1.3	0.2
GAN	−34.7	−3.1	−5.4	2.7	1.7	**−0.6**	4.5	−5.0	3.4	−5.9	−3.4	−3.6	−2.9	1.7	11.7	−0.7
HAN	−35.0	−14.4	−17.0	−8.6	−10.7	−14.8	−6.6	−16.4	−10.0	−10.4	−7.7	−8.7	−8.4	−10.4	**1.0**	−5.5
KDO	−37.5	−9.2	−15.1	−4.2	−7.3	−7.4	**−3.5**	−13.2	−3.5	−9.6	−7.2	−8.1	−7.5	−5.4	4.2	−5.1
MIY	−23.7	−14.2	−15.2	−9.0	−7.4	−6.1	−6.4	−13.5	−5.6	−5.1	−5.3	−4.3	−4.6	−8.7	−5.9	**−3.6**
MLE	−40.1	−12.0	−10.5	−5.8	−6.4	−9.3	−2.6	−10.8	−5.0	−10.9	−7.9	−8.7	−7.9	−9.4	**1.1**	−5.4
TOW	−17.5	2.5	−22.0	10.7	−4.3	1.3	−7.2	−8.9	**−1.1**	−3.5	−4.7	−3.8	−4.6	−2.5	3.0	−2.7
Köppen-Geiger climate B																
ADE	−12.2	−1.8	−20.4	4.8	−6.6	−0.4	−10.9	−11.0	−4.3	−4.5	−8.0	−5.3	−7.9	**−0.1**	−0.5	−3.4
ADR	−10.6	−29.2	−49.8	−21.5	−40.4	−26.5	−38.1	−41.5	−15.6	−10.9	−14.1	−11.6	−14.0	−31.5	−32.3	**−8.1**
ALB	−10.9	10.0	−51.3	29.7	−17.8	7.8	−33.6	−21.1	2.6	**0.3**	−6.8	0.7	−6.1	4.2	4.0	1.8
ARI	−13.7	9.4	−43.8	24.3	−18.2	6.4	−24.2	−15.3	2.2	−5.5	−10.5	−6.3	−10.3	−1.3	**−0.9**	−4.8
BRO	−7.5	16.6	−14.6	25.5	7.2	8.3	4.0	2.3	7.7	3.6	**−0.2**	3.7	0.9	19.1	14.4	4.8
GAB	−7.2	10.2	−18.9	18.6	1.0	2.2	−7.8	−4.3	**0.9**	−1.9	−7.4	−2.6	−7.4	7.1	4.9	−3.7
HAF	−9.3	9.4	−43.7	21.8	−16.1	**−2.0**	−24.7	−16.5	−5.5	−5.5	−11.3	−6.3	−10.8	3.9	2.7	−4.2
JOR	**−0.7**	−6.4	−50.5	8.4	−32.8	−12.3	−38.1	−28.8	1.4	−7.5	−13.2	−8.3	−13.2	−18.4	−18.8	−4.7
LAS	−18.3	**−0.3**	−46.2	12.1	−24.5	−4.6	−29.8	−22.2	−8.4	−12.3	−17.4	−13.2	−16.9	−8.1	−7.2	−11.0
LOY	−8.8	5.2	−32.3	11.3	−9.5	**−3.2**	−15.0	−12.8	−5.9	−4.4	−9.7	−5.3	−9.5	5.5	3.9	−5.4
MIS	−15.7	−8.2	−42.6	**4.9**	−27.2	−8.6	−32.5	−26.7	−11.9	−12.7	−17.0	−12.9	−16.6	−14.2	−14.4	−10.8
OUJ	−15.6	−7.5	−24.6	**2.2**	−17.5	−11.8	−20.1	−16.8	−14.2	−10.3	−14.5	−10.7	−14.2	−9.8	−10.8	−8.9
PAN	−17.6	−7.1	−18.0	**−0.2**	−4.9	−2.1	−5.4	−10.6	−0.3	−1.2	−3.5	−0.7	−2.0	−0.5	−1.7	−3.4
POR	−3.5	6.2	−10.2	10.7	5.8	3.4	0.7	−2.0	**0.4**	0.9	−3.3	0.7	−2.8	10.2	9.0	0.8
RVD	1.6	26.8	−41.8	45.9	−10.0	12.5	−21.5	−5.3	10.5	1.6	−4.5	**0.8**	−4.4	7.7	4.6	3.8
SAL	−11.6	**0.1**	−41.5	11.1	−17.0	0.2	−25.1	−20.3	−4.6	−3.3	−8.4	−3.3	−7.4	0.5	0.3	−1.6
SHA	6.2	−20.8	−44.2	−10.7	−35.4	−21.5	−31.0	−32.8	−2.7	−3.9	−6.5	−4.5	−6.8	−31.3	−33.6	**0.8**
SRR	−8.1	3.1	−19.8	15.2	−6.1	6.5	−14.2	−7.7	1.2	1.7	−4.0	**0.9**	−4.0	4.2	5.4	−1.4
TAB	−15.0	1.3	−21.5	12.6	−11.2	**1.1**	−12.7	−10.5	−2.7	−6.0	−9.5	−6.2	−9.3	−2.5	−2.8	−4.4
TAT	3.4	−8.7	−38.7	0.9	−23.4	−16.1	−25.9	−24.0	2.4	−2.3	−7.6	−2.5	−7.5	−9.6	−11.6	**−0.6**
WAG	−6.5	9.3	−19.1	19.2	−0.8	6.4	−8.6	−3.3	2.9	2.8	−1.7	1.3	−2.4	6.8	6.5	**0.5**
Köppen-Geiger climate C																
CAH	−23.9	−11.2	−9.9	−7.4	−3.6	−4.2	**−0.5**	−8.0	−3.3	−4.2	−3.0	−3.4	−2.3	−0.7	−2.0	−3.8
CAP	−13.0	−10.0	−16.9	−5.6	−6.6	−4.9	−9.8	−11.8	−5.6	−5.1	−3.7	−6.1	−4.1	**−2.3**	−3.5	−6.2
CAS	−12.4	−3.0	−22.4	5.9	−8.6	−1.4	−9.6	−11.6	0.4	0.4	2.3	0.5	2.3	**−0.1**	2.1	0.1
CHB	−28.8	−22.5	−23.4	−18.6	−19.0	−15.4	−16.3	−21.4	−15.4	−16.9	−16.9	−16.0	−16.2	−17.9	−17.3	**−14.0**
CHL	−4.1	3.9	4.2	10.2	14.2	6.7	10.7	5.9	8.9	6.5	12.0	5.9	12.4	8.4	9.7	**−0.2**
CHO	−6.7	2.6	**0.2**	10.5	9.9	4.0	5.7	2.9	1.6	1.6	7.2	0.9	7.5	5.1	6.1	−3.2
DUR	−9.8	0.3	−11.1	5.6	1.1	**0.0**	−1.0	−4.3	2.0	−0.4	2.2	−0.4	2.2	4.4	5.1	−0.4
FUU	−17.7	−15.8	−14.4	−12.2	−10.8	−10.7	−9.5	−12.9	−10.7	−8.5	**−7.5**	−8.7	−7.8	−11.0	−11.5	−8.3
JAE	−13.2	**−0.0**	−18.9	10.5	−10.5	−3.5	−14.6	−10.1	−6.7	−6.6	−4.5	−7.0	−4.6	−4.3	−2.3	−6.1
KAA	−10.0	−2.1	−0.8	3.9	8.4	2.0	6.6	0.2	4.1	0.3	5.4	**−0.0**	7.0	5.3	6.3	−2.8
KAO	−9.9	−1.0	−1.9	5.9	6.5	1.0	4.2	**0.0**	−1.5	−1.6	2.9	−1.9	3.8	4.3	5.4	−2.4
KAS	−18.9	−8.7	−21.2	3.4	−8.0	−3.9	−13.1	−16.4	−2.2	−7.4	−4.7	−7.2	−3.3	**2.1**	2.9	−3.8
KWA	−16.7	−2.5	−6.3	3.0	−2.3	−0.4	**0.2**	−3.4	1.2	−4.7	−4.0	−4.5	−3.9	−2.1	−1.5	−2.5
LOC	−12.8	−0.6	−15.4	7.4	−6.2	5.5	−4.0	−8.1	5.9	−0.7	−1.5	0.4	**−0.2**	−1.1	1.8	3.9
LUS	−10.4	−3.7	−8.6	5.8	**0.4**	−1.4	−3.2	−5.2	0.6	−1.4	1.8	−2.2	2.0	3.3	3.4	−2.3
MEL	−8.3	−1.8	−10.3	5.6	−0.4	2.4	−4.0	−3.9	2.3	−0.5	0.8	−1.6	**0.2**	2.3	1.9	−1.9
MIL	−18.3	−7.6	−15.5	**−0.5**	−9.2	−7.0	−8.6	−10.7	−5.9	−6.3	−4.9	−6.0	−4.5	−4.9	−2.2	−5.2
MUT	−4.0	3.4	3.5	8.7	14.3	6.3	11.5	3.7	8.7	4.9	11.6	4.7	12.6	10.1	12.5	**1.8**
MZU	−13.6	−6.7	−24.8	3.4	−6.3	−1.4	−12.1	−15.2	**−0.2**	−2.2	0.8	−3.1	1.3	5.1	4.2	−2.4
ORE	−10.0	−1.7	−12.8	6.0	−4.4	1.9	−3.9	−4.4	0.9	−1.8	−1.2	−1.5	−0.9	1.3	2.6	**−0.2**
PRE	−8.8	5.2	−18.1	14.2	−1.1	1.5	−8.5	−5.5	−0.8	0.9	6.3	**−0.1**	5.4	1.2	2.7	−3.6
ROC	−15.4	1.6	−15.8	12.1	**−0.3**	6.3	−2.9	−5.4	8.6	1.4	3.2	0.5	2.2	4.2	3.4	−1.6
SEA	−5.6	3.7	−23.0	13.5	−3.4	3.5	−8.6	−9.8	2.8	**1.2**	4.6	1.7	5.7	11.9	14.2	4.7
STE	−3.1	16.6	−21.8	27.1	2.8	10.1	−6.5	**−1.0**	7.4	3.6	6.5	2.2	5.7	9.4	10.9	2.2
STR	−15.1	−5.3	−19.2	1.6	−7.8	−0.9	−9.7	−11.8	−0.7	−1.2	−0.6	−1.0	−0.2	−0.9	**−0.1**	−0.7
VUW	−4.6	3.6	−5.6	9.2	7.4	5.4	3.3	**−0.1**	2.1	1.3	6.0	1.1	6.1	7.1	8.8	2.2
Köppen-Geiger climate D																
BIS	−11.4	−3.3	−35.0	5.4	−16.6	−2.9	−21.6	−18.9	−2.8	−0.9	−0.4	−1.0	−0.5	5.0	0.7	**−0.3**
DAO	−10.3	−8.0	−18.6	4.4	−9.6	**−0.9**	−16.9	−13.5	−2.5	−6.0	−7.7	−4.5	−5.0	1.7	−2.6	−3.8
KAZ	−12.9	−11.3	−35.7	2.4	−19.0	−2.9	−26.9	−24.8	−4.6	−4.9	−6.7	−4.5	−5.0	1.5	**−1.3**	−3.5
KIR	−10.4	−9.6	−11.8	−3.3	−8.3	−2.1	−9.6	−9.4	−5.4	−4.5	−6.2	−4.9	−5.2	**−0.9**	−1.6	−5.1
LYN	−9.8	−7.3	−15.0	3.5	−7.4	−5.2	−10.0	−9.2	−5.9	**−0.7**	1.0	−1.1	0.9	4.5	1.3	−2.4
MAD	−13.1	−2.0	−22.2	5.6	−7.5	1.6	−11.1	−11.6	1.3	0.4	0.7	**0.2**	1.0	6.3	3.0	−0.2
NOR	−10.7	−5.9	−6.0	1.1	−3.2	1.0	−3.1	−3.7	−1.0	−2.2	−3.2	−3.0	−3.2	2.1	**0.7**	−3.6
ODE	−8.4	4.4	−14.6	19.8	−8.1	2.0	−18.1	−7.0	3.9	0.6	0.8	**−0.4**	2.1	12.2	5.4	−1.1
VIS	−11.0	−3.3	−8.4	2.2	−5.7	0.5	−4.3	−4.3	−0.5	−2.3	−2.6	−3.2	−3.0	2.4	**0.0**	−2.5

Table A.8
Same as Table A.5 but for RMSE and the INDEP dataset.

Site	P2	E2	PB	AB	S3	Y4	M1	M2	Y5	G1	G2	G3	G4	N1	N2	N3
Köppen-Geiger climate A																
CHI	41.7	38.0	32.1	40.2	30.4	31.1	29.6	30.4	29.6	30.5	30.3	29.2	28.7	23.2	26.1	**23.1**
DAR	43.9	37.0	31.0	34.2	28.5	28.5	27.4	29.9	26.7	26.0	25.3	24.8	24.0	22.3	22.5	**21.0**
FEN	38.6	36.7	24.0	32.6	22.6	32.9	19.9	25.0	22.9	21.9	20.8	21.0	19.8	23.1	22.9	**18.0**
GAN	61.4	39.4	34.9	39.0	31.7	33.5	31.0	35.1	33.6	31.8	31.0	29.3	29.2	27.4	32.7	**26.5**
HAN	57.5	37.9	34.5	35.7	30.1	34.9	26.1	35.0	30.9	28.4	26.8	26.1	25.8	28.2	26.4	**23.8**
KDO	62.2	39.0	36.1	37.4	31.1	34.8	29.4	36.0	32.5	31.5	30.2	29.2	28.8	28.4	29.0	**27.3**
MIY	45.4	40.7	35.4	39.1	29.1	33.3	27.5	34.3	31.9	27.2	27.7	26.0	26.6	26.2	25.4	**23.2**
MLE	66.2	38.8	36.0	36.7	31.0	34.4	28.8	36.1	31.8	31.4	29.6	27.9	27.3	29.0	28.0	**24.9**
TOW	45.1	43.6	46.3	45.3	32.2	32.8	33.9	39.4	33.3	30.0	30.4	28.5	29.1	25.1	25.5	**23.4**
Köppen-Geiger climate B																
ADE	34.6	40.9	45.3	44.6	30.8	31.1	34.0	39.1	32.4	26.7	28.0	26.1	27.3	25.4	23.2	**23.1**
ADR	34.6	54.5	68.9	52.1	58.8	53.6	55.9	62.5	41.2	30.3	32.6	30.3	32.1	46.8	49.6	**28.3**
ALB	39.7	47.6	74.3	68.4	44.0	43.0	54.6	51.5	41.5	33.4	32.8	32.9	31.9	29.6	29.7	**26.9**
ARI	39.8	45.4	60.2	56.6	36.2	34.4	42.3	41.1	34.8	28.9	30.4	27.6	28.9	26.0	24.6	**22.8**
BRO	46.6	48.5	41.4	52.2	35.3	34.2	33.0	37.3	34.9	29.3	28.3	28.0	27.9	40.7	34.6	**24.8**
GAB	39.6	45.2	43.3	48.1	32.8	32.6	32.3	36.3	32.7	30.4	30.8	30.2	30.3	29.5	26.7	**24.5**
HAF	34.0	41.4	62.1	48.1	34.9	32.0	41.4	41.8	33.1	27.7	29.3	27.1	28.7	24.2	**23.5**	23.9
JOR	31.3	47.7	73.2	54.2	53.5	44.1	56.5	56.1	40.6	28.4	30.3	28.3	30.0	39.2	41.6	**25.6**
LAS	48.1	50.0	70.9	53.7	51.3	45.4	57.2	54.0	46.0	43.9	45.7	43.1	44.5	40.9	40.6	**38.9**
LOY	42.6	48.1	62.8	48.2	42.5	37.6	45.3	48.1	39.2	32.3	33.5	31.8	32.9	34.8	31.9	**28.1**
MIS	42.2	50.0	68.5	53.9	51.2	46.2	54.5	56.1	45.3	37.3	39.0	36.2	37.9	39.2	41.5	**31.7**
OUJ	37.5	45.0	46.8	46.4	39.1	40.8	38.2	43.0	40.0	30.6	32.5	29.7	31.9	31.4	34.0	**26.1**
PAN	44.3	39.3	37.9	37.2	28.3	29.1	28.2	33.0	28.7	27.0	26.8	25.9	26.6	26.8	25.2	**22.3**
POR	42.6	47.6	44.2	49.0	38.7	36.5	37.0	41.6	37.9	32.4	32.1	31.7	31.5	36.8	33.7	**28.4**
RVD	35.8	57.1	62.7	76.0	37.0	39.9	43.1	43.5	41.3	29.0	29.2	28.1	28.3	30.5	27.7	**25.7**
SAL	33.8	38.9	60.9	47.9	36.2	34.4	42.7	42.3	34.1	26.9	28.2	26.0	26.9	24.7	24.2	**22.3**
SHA	23.4	33.7	57.0	31.4	47.1	38.8	42.1	45.1	24.4	22.2	22.8	21.9	23.2	39.8	43.7	**20.5**
SRR	37.5	43.2	46.9	52.9	34.6	37.1	39.2	38.4	35.6	32.1	32.4	30.0	30.3	27.9	27.2	**24.8**
TAB	39.1	43.6	48.3	49.0	36.5	37.9	37.8	41.4	37.2	30.3	31.3	28.9	30.0	28.8	29.8	**25.0**
TAT	31.4	44.9	61.0	43.1	45.5	42.0	45.2	49.7	36.7	25.9	26.8	25.1	26.5	30.1	31.0	**21.4**
WAG	36.3	45.8	47.4	52.7	33.1	33.3	34.7	39.0	33.2	29.3	29.0	27.9	27.9	28.4	26.0	**24.0**
Köppen-Geiger climate C																
CAH	46.3	37.9	32.9	35.7	28.3	30.9	27.4	31.9	29.8	26.6	26.4	25.1	25.4	25.1	24.9	**22.9**
CAP	37.4	43.3	45.1	43.9	32.2	33.9	35.5	41.4	34.5	29.8	29.0	29.2	28.4	**26.0**	27.0	26.9
CAS	37.1	40.3	47.6	40.1	33.2	32.1	34.1	39.0	32.1	27.0	27.2	25.5	25.8	26.0	26.1	**21.6**
CHB	48.8	41.8	39.8	38.3	33.7	33.1	30.7	37.7	31.2	30.9	31.6	29.7	30.5	32.2	31.3	**26.6**
CHL	42.6	41.5	32.7	42.7	35.2	32.6	31.7	31.5	32.0	34.9	37.9	34.3	38.3	27.7	30.2	**26.1**
CHO	43.8	43.2	32.6	45.1	32.8	32.5	29.7	32.0	31.3	33.4	35.5	32.9	35.8	26.6	28.2	**26.4**
DUR	41.6	41.3	36.8	41.4	29.0	30.0	28.4	33.8	30.3	27.6	27.9	26.5	27.2	25.0	27.0	**23.1**
FUU	38.9	40.1	35.3	37.3	29.2	32.3	28.5	34.2	30.4	24.9	24.4	24.3	23.8	26.3	26.7	**22.3**
JAE	36.2	44.7	42.2	48.2	35.1	36.6	36.0	39.2	36.7	30.0	28.6	28.6	27.4	29.3	28.5	**24.8**
KAA	44.0	40.4	31.5	41.9	30.6	30.9	28.5	30.8	30.1	32.5	34.1	32.2	34.5	25.2	27.0	**24.8**
KAO	43.0	40.3	31.3	42.4	29.4	30.6	27.6	30.6	29.8	30.7	31.8	30.3	31.8	24.6	26.1	**24.3**
KAS	45.8	41.1	45.3	46.0	32.1	34.0	35.3	41.1	32.0	32.6	32.4	31.3	30.4	25.7	26.5	**25.6**
KWA	43.2	40.8	34.0	41.6	26.8	32.9	27.8	32.4	33.1	27.3	26.8	26.3	25.9	22.9	23.6	**22.6**
LOC	41.5	42.0	40.8	45.1	32.8	38.8	31.9	37.3	38.1	28.3	28.4	26.6	26.8	27.9	27.3	**24.3**
LUS	38.6	38.1	31.8	42.6	26.4	29.4	26.7	29.3	27.5	28.7	28.9	28.3	28.7	24.0	24.5	**23.0**
MEL	32.7	39.1	38.4	43.4	28.2	28.7	29.6	33.5	29.3	25.5	25.6	24.2	24.5	21.8	21.9	**21.1**
MIL	41.6	42.1	41.6	40.9	33.2	36.3	33.0	38.8	34.9	28.7	27.9	27.3	26.7	26.5	26.1	**24.2**
MUT	46.1	42.7	34.4	43.6	37.4	34.9	34.5	33.5	34.4	37.8	41.2	37.5	41.6	29.8	33.5	**28.0**
MZU	42.0	41.4	46.9	44.2	31.6	32.9	34.8	39.7	31.2	31.4	31.5	30.7	30.4	26.1	26.5	**25.7**
ORE	32.7	39.3	36.6	42.5	27.2	30.2	27.8	32.2	32.4	25.9	25.4	25.2	24.2	23.0	23.6	**22.2**
PRE	36.6	42.0	40.0	44.1	29.4	30.1	29.7	32.1	29.3	28.8	30.1	27.8	29.5	24.2	24.3	**23.1**
ROC	43.4	41.6	41.9	44.3	30.1	31.6	31.2	35.6	32.6	29.0	29.7	27.3	28.1	24.7	24.1	**21.9**
SEA	39.7	45.2	55.2	49.3	38.0	36.0	42.1	46.3	37.1	31.3	32.2	30.6	31.7	30.5	33.3	**26.1**
STE	37.3	51.8	47.6	58.1	35.9	36.0	36.1	40.5	36.9	31.3	32.3	30.0	31.1	29.4	30.7	**27.2**
STR	39.7	35.4	39.5	37.1	27.5	29.4	29.0	33.6	28.9	24.5	24.5	23.2	23.3	22.1	21.8	**20.3**
VUW	45.1	46.7	41.7	47.0	42.1	40.6	39.8	38.4	39.1	38.8	41.3	38.7	41.1	37.4	41.1	**36.8**
Köppen-Geiger climate D																
BIS	35.3	40.0	56.8	42.7	36.5	34.0	41.5	43.4	34.0	26.9	26.6	26.3	25.8	25.7	25.5	**22.5**
DAO	36.3	40.7	42.4	51.9	34.7	34.9	41.7	39.3	35.1	30.0	31.2	27.4	28.4	25.9	24.7	**22.2**
KAZ	40.8	47.1	60.8	54.6	45.3	41.5	51.6	51.7	41.4	34.9	35.3	33.2	33.8	30.4	29.9	**27.8**
KIR	31.9	35.3	36.2	39.1	30.0	28.2	32.5	33.4	28.8	25.5	26.3	24.5	24.9	21.8	21.8	**20.7**
LYN	38.7	43.2	44.0	43.6	34.3	33.4	36.2	39.8	33.2	29.7	29.6	28.6	28.9	29.1	27.2	**24.8**
MAD	37.1	37.6	45.3	41.6	30.4	31.5	33.4	36.7	31.6	26.0	25.4	24.9	24.3	24.4	23.2	**21.3**
NOR	34.5	37.6	33.9	39.8	28.6	30.6	28.6	31.3	30.3	27.4	27.3	26.2	26.2	23.5	22.9	**22.0**
ODE	43.8	55.7	52.5	65.0	44.4	45.9	50.1	50.3	46.8	38.2	38.6	36.7	37.2	37.8	35.1	**31.3**
VIS	35.8	40.7	39.2	41.5	31.7	34.5	32.5	36.4	35.1	28.7	28.4	27.6	27.5	25.7	25.4	**24.5**

Data availability

Data will be made available on request.

References

[1] J.A. Ruiz-Arias, C.A. Gueymard, Solar resource for high-concentrator photovoltaic applications, in: High Concentrator Photovoltaics, Springer International Publishing, 2015, pp. 261–302, http://dx.doi.org/10.1007/978-3-319-15039-0_10.

[2] N. Janotte, S. Wilbert, F. Sallaberry, M. Schroedter-Homscheidt, L. Ramirez, Principles of CSP performance assessment, in: The Performance of Concentrated Solar Power (CSP) Systems, Elsevier, 2017, pp. 31–64, http://dx.doi.org/10.1016/b978-0-08-100447-0.00002-x.

[3] M.J. Mayer, Influence of design data availability on the accuracy of physical photovoltaic power forecasts, Sol. Energy 227 (2021) 532–540, http://dx.doi.org/10.1016/j.solener.2021.09.044.

[4] M.J. Mayer, G. Gróf, Extensive comparison of physical models for photovoltaic power forecasting, Appl. Energy 283 (2021) 116239, http://dx.doi.org/10.1016/j.apenergy.2020.116239.

[5] M. Manni, A. Nocente, M. Bellmann, G. Lobaccaro, Multi-stage validation of a solar irradiance model chain: An application at high latitudes, Sustain. Sci. 15 (4) (2023) 2938, http://dx.doi.org/10.3390/su15042938.

[6] B.M. Lopes, A.M. Costa, W. Uturbey, Simulation with performance evaluation of photovoltaic production using long term monthly irradiation data, Renew. Energy 223 (2024) 120021, http://dx.doi.org/10.1016/j.renene.2024.120021.

[7] M. Sengupta, A. Habte, S. Wilbert, C. Gueymard, J. Remund, E. Lorenz, W. van Sark, A.R. Jensen, Best Practices Handbook for the Collection and Use of Solar Resource Data for Solar Energy Applications: Fourth Edition, Technical Report, National Renewable Energy Laboratory (NREL), Golden, CO (United States), 2024, http://dx.doi.org/10.2172/2448063, URL: https://www.osti.gov/biblio/2448063.

[8] R. Perez, T. Cebecauer, M. Súri, Semi-empirical satellite models, in: J. Kleissl (Ed.), Solar Energy Forecasting and Resource Assessment, Elsevier, 2013, pp. 21–48, http://dx.doi.org/10.1016/B978-0-12-397177-7.00002-4.

[9] E.F. Abreu, C.A. Gueymard, P. Canhoto, M.J. Costa, Performance assessment of clear-sky solar irradiance predictions using state-of-the-art radiation models and input atmospheric data from reanalysis or ground measurements, Sol. Energy 252 (2023) 309–321, http://dx.doi.org/10.1016/j.solener.2023.01.051.

[10] C.A. Gueymard, J.A. Ruiz-Arias, Extensive worldwide validation and climate sensitivity analysis of direct irradiance predictions from 1-min global irradiance, Sol. Energy 128 (2016) 1–30, http://dx.doi.org/10.1016/j.solener.2015.10.010, Publisher: Elsevier.

[11] F.P. Kreuwel, W.H. Knap, L.R. Visser, W.G. van Sark, J. Vilà-Guerau de Arellano, C.C. van Heerwaarden, Analysis of high frequency photovoltaic solar energy fluctuations, Sol. Energy 206 (2020) 381–389, http://dx.doi.org/10.1016/j.solener.2020.05.093.

[12] M. Lave, M.J. Reno, R.J. Broderick, Characterizing local high-frequency solar variability and its impact to distribution studies, Sol. Energy 118 (2015) 327–337, http://dx.doi.org/10.1016/j.solener.2015.05.028.

[13] C.A. Gueymard, Cloud and albedo enhancement impacts on solar irradiance using high-frequency measurements from thermopile and photodiode radiometers. Part 1: Impacts on global horizontal irradiance, Sol. Energy 153 (2017) 755–765, http://dx.doi.org/10.1016/j.solener.2017.05.004.

[14] R. Blaga, The impact of temporal smoothing on the accuracy of separation models, Sol. Energy 191 (2019) 371–381, http://dx.doi.org/10.1016/j.solener.2019.08.078.

[15] M. Zamora Zapata, K. Lappalainen, A. Kankiewicz, J. Kleissl, Comparing solar inverter design rules to subhourly solar resource simulations, J. Renew. Sustain. Energy 15 (5) (2023) http://dx.doi.org/10.1063/5.0151042.

[16] N.A. Engerer, Minute resolution estimates of the diffuse fraction of global irradiance for southeastern Australia, Sol. Energy 116 (2015) 215–237, http://dx.doi.org/10.1016/j.solener.2015.04.012.

[17] H. Suehrcke, P. McCormick, The diffuse fraction of instantaneous solar radiation, Sol. Energy 40 (5) (1988) 423–430, http://dx.doi.org/10.1016/0038-092x(88)90097-7.

[18] D. Yang, Estimating 1-min beam and diffuse irradiance from the global irradiance: A review and an extensive worldwide comparison of latest separation models at 126 stations, Renew. Sustain. Energ. Rev. 159 (2022) 112195, http://dx.doi.org/10.1016/j.rser.2022.112195, Publisher: Elsevier.

[19] J.A. Ruiz-Arias, C.A. Gueymard, Solar irradiance component separation benchmarking: The critical role of dynamically-constrained sky conditions, Renew. Sustain. Energy Rev. 202 (2024) 114678, http://dx.doi.org/10.1016/j.rser.2024.114678.

[20] R. Aler, I.M. Galván, J.A. Ruiz-Arias, C.A. Gueymard, Improving the separation of direct and diffuse solar radiation components using machine learning by gradient boosting, Sol. Energy 150 (2017) 558–569, http://dx.doi.org/10.1016/j.solener.2017.05.018.

[21] C.G. Tianqi Chen, XGBoost: A scalable tree boosting system, Proc. 22nd ACM SIGKDD Int. Conf. on Knowl. Discov. Data Min. (2016) 785–794, http://dx.doi.org/10.1145/2939672.2939785.

[22] R.A. Ramadhan, Y.R. Heatubun, S.F. Tan, H.-J. Lee, Comparison of physical and machine learning models for estimating solar irradiance and photovoltaic power, Renew. Energy 178 (2021) 1006–1019, http://dx.doi.org/10.1016/j.renene.2021.06.079.

[23] R.A. Rajagukguk, H. Lee, Enhancing the performance of solar radiation decomposition models using deep learning, J. Sol. Energy Soc. India 43 (3) (2023) 73–86, http://dx.doi.org/10.7836/kses.2023.43.3.073.

[24] H.L. Rial A. Rajagukguk, Application of explainable machine learning for estimating direct and diffuse components of solar irradiance, Sci. Rep. 15 (1) (2025) http://dx.doi.org/10.1038/s41598-025-91158-x.

[25] M. Oh, C.K. Kim, B. Kim, C. Yun, J.Y. Kim, Y. Kang, H.G. Kim, Analysis of minute-scale variability for enhanced separation of direct and diffuse solar irradiance components using machine learning algorithms, Energy 241 (2022) http://dx.doi.org/10.1016/j.energy.2021.122921.

[26] E. Rodríguez, L. Cornejo-Ponce, J.M. Cardemil, A.R. Starke, E.L. Droguett, Estimation of one-minute direct normal irradiance using a deep neural network for five climate zones, Renew. Sustain. Energy Rev. 183 (2023) http://dx.doi.org/10.1016/j.rser.2023.113486.

[27] D. Yang, Y. Gu, M.J. Mayer, C.A. Gueymard, W. Wang, J. Kleissl, M. Li, Y. Chu, J.M. Bright, Regime-dependent 1-min irradiance separation model with climatology clustering, Renew. Sustain. Energy Rev. 189 (2024) http://dx.doi.org/10.1016/j.rser.2023.113992.

[28] J.A. Ruiz-Arias, C.A. Gueymard, GISPLIT: High-performance global solar irradiance component-separation model dynamically constrained by 1-min sky conditions, Sol. Energy 269 (2024) http://dx.doi.org/10.1016/j.solener.2024.112363.

[29] J. Ruiz-Arias, C. Gueymard, CAELUS: Classification of sky conditions from 1-min time series of global solar irradiance using variability indices and dynamic thresholds, Sol. Energy 263 (2023) http://dx.doi.org/10.1016/j.solener.2023.111895.

[30] Y. Chu, D. Yang, H. Yu, X. Zhao, M. Li, Can end-to-end data-driven models outperform traditional semi-physical models in separating 1-min irradiance? Appl. Energy 356 (2024) 122434, http://dx.doi.org/10.1016/j.apenergy.2023.122434.

[31] S. Mengmeng, Y. Dazhi, L. Bai, F. Disong, S. Hongrong, X. Xiang'ao, M. János Mayer, Solar irradiance separation with deep learning: An interpretable multi-task and physically constrained model based on individual–interactive features, Sol. Energy 290 (2025) 113353, http://dx.doi.org/10.1016/j.solener.2025.113353.

[32] A. Driemel, J. Augustine, K. Behrens, S. Colle, C. Cox, E. Cuevas-Agulló, F.M. Denn, T. Duprat, M. Fukuda, H. Grobe, M. Haeffelin, G. Hodges, N. Hyett, O. Ijima, A. Kallis, W. Knap, V. Kustov, C.N. Long, D. Longenecker, A. Lupi, M. Maturilli, M. Mimouni, L. Ntsangwane, H. Ogihara, X. Olano, M. Olefs, M. Omori, L. Passamani, E. Bueno Pereira, H. Schmithüsen, S. Schumacher, R. Sieger, J. Tamlyn, R. Vogt, L. Vuilleumier, X. Xia, A. Ohmura, G. König-Langlo, Baseline surface radiation network (BSRN): Structure and data description (1992–2017), Earth Syst. Sci. Data 10 (3) (2018) 1491–1501, http://dx.doi.org/10.5194/essd-10-1491-2018.

[33] A. Forstinger, Y.-M. Saint-Drenan, S. Wilbert, A. Jensen, B. Kraas, C. Fernández Peruchena, C. Gueymard, D. Ronzio, D. Yang, E. Collino, J. Polo Martinez, J. Ruiz-Arias, N. Hanrieder, P. Blanc, IEA-PVPS task-16 reference solar measurements. MINES ParisTech, 2021, http://dx.doi.org/10.23646/3491b1a6-e32d-4b34-9dbb-ee0affe49e36.

[34] C.A. Gueymard, A review of validation methodologies and statistical performance indicators for modeled solar radiation data: Towards a better bankability of solar projects, Renew. Sustain. Energy Rev. 39 (2014) 1024–1034, http://dx.doi.org/10.1016/j.rser.2014.07.117, URL: https://linkinghub.elsevier.com/retrieve/pii/S1364032114005693.

[35] I. Goodfellow, Y. Bengio, A. Courville, Deep Learning, MIT Press, MIT Press, 2016.

[36] R.H. Inman, H.T. Pedro, C.F. Coimbra, Solar forecasting methods for renewable energy integration, Prog. Energy Combust. Sci. 39 (6) (2013) 535–576, http://dx.doi.org/10.1016/j.pecs.2013.06.002, URL: https://www.sciencedirect.com/science/article/pii/S0360128513000294.

[37] E. Rodríguez, L. Cornejo-Ponce, J.M. Cardemil, A.R. Starke, E.L. Droguett, Estimation of one-minute direct normal irradiance using a deep neural network for five climate zones, Renew. Sustain. Energy Rev. 183 (2023) 113486, http://dx.doi.org/10.1016/j.rser.2023.113486.

[38] O. Bamisile, A. Oluwasanmi, C. Ejiyi, N. Yimen, S. Obiora, Q. Huang, Comparison of machine learning and deep learning algorithms for hourly global/diffuse solar radiation predictions, Int. J. Energy Res. (2021) er.6529, http://dx.doi.org/10.1002/er.6529, URL: https://onlinelibrary.wiley.com/doi/10.1002/er.6529.

[39] P. Kumari, D. Toshniwal, Deep learning models for solar irradiance forecasting: A comprehensive review, J. Clean. Prod. 318 (2021) 128566, http://dx.doi.org/10.1016/j.jclepro.2021.128566, URL: https://linkinghub.elsevier.com/retrieve/pii/S0959652621027736.

[40] M. Ajith, M. Martínez-Ramón, Deep learning based solar radiation micro forecast by fusion of infrared cloud images and radiation data, Appl. Energy 294 (2021) http://dx.doi.org/10.1016/j.apenergy.2021.117014.

[41] H.E. Beck, N.E. Zimmermann, T.R. McVicar, N. Vergopolan, A. Berg, E.F. Wood, Present and future Köppen–Geiger climate classification maps at 1-km resolution, Sci. Data 5 (1) (2018) http://dx.doi.org/10.1038/sdata.2018.214.

[42] J.A. Ruiz-Arias, SPARTA: Solar parameterization for the radiative transfer of the cloudless atmosphere, Renew. Sustain. Energy Rev. 188 (2023) 113833, http://dx.doi.org/10.1016/j.rser.2023.113833.

[43] M.J. Blanco, K. Milidonis, A.M. Bonanos, Updating the PSA sun position algorithm, Sol. Energy 212 (2020) 339–341, http://dx.doi.org/10.1016/j.solener.2020.10.084.

[44] R. Perez, P. Ineichen, K. Moore, M. Kmiecik, C. Chain, R. George, F. Vignola, A new operational model for satellite-derived irradiances: description and validation, Sol. Energy 73 (5) (2002) 307–317, http://dx.doi.org/10.1016/s0038-092x(02)00122-6.

[45] E. Paulescu, R. Blaga, A simple and reliable empirical model with two predictors for estimating 1-minute diffuse fraction, Sol. Energy 180 (2019) 75–84, http://dx.doi.org/10.1016/j.solener.2019.01.029.

[46] E.F. Abreu, P. Canhoto, M.J. Costa, Prediction of diffuse horizontal irradiance using a new climate zone model, Renew. Sustain. Energy Rev. 110 (2019) 28–42, http://dx.doi.org/10.1016/j.rser.2019.04.055.

[47] A.R. Starke, L.F. Lemos, C.M. Barni, R.D. Machado, J.M. Cardemil, J. Boland, S. Colle, Assessing one-minute diffuse fraction models based on worldwide climate features, Renew. Energy 177 (2021) 700–714, http://dx.doi.org/10.1016/j.renene.2021.05.108.

[48] E. Paulescu, M. Paulescu, Minute-scale models for the diffuse fraction of global solar radiation balanced between accuracy and accessibility, Appl. Sci. (Switzerland) 13 (11) (2023) http://dx.doi.org/10.3390/app13116558.

[49] J.M. Bright, N.A. Engerer, Engerer2: Global re-parameterisation, update, and validation of an irradiance separation model at different temporal resolutions, J. Renew. Sustain. Energy 11 (3) (2019) http://dx.doi.org/10.1063/1.5097014.

[50] X. Sun, J.M. Bright, C.A. Gueymard, B. Acord, P. Wang, N.A. Engerer, Worldwide performance assessment of 75 global clear-sky irradiance models using principal component analysis, Renew. Sustain. Energy Rev. 111 (2019) 550–570, http://dx.doi.org/10.1016/j.rser.2019.04.006.

[51] X. Sun, J.M. Bright, C.A. Gueymard, X. Bai, B. Acord, P. Wang, Worldwide performance assessment of 95 direct and diffuse clear-sky irradiance models using principal component analysis, Renew. Sustain. Energy Rev. 135 (2021) 110087, http://dx.doi.org/10.1016/j.rser.2020.110087.